ADVANCED MATERIALS INTERFACES
Open Access
www.advmatinterfaces.de

High-throughput Photocatalytic Reactor With *in Operando* Characterisation for Fast Screening of Materials for the Photodegradation of Water-Borne Pollutants

*Elisante Maloda Maloda, Likius Shipwiisho Daniel, Dmitry Busko, Andrey Turshatov, Justine Sageka Nyarige, and Bryce Sydney Richards**

A novel fast-screening photocatalytic reactor system (FaS-PhoReS) using simulated terrestrial sunlight is conceived and demonstrated. The instrument is capable of screening, automated data measurement and recording 32 samples at once with no external characterisation devices (e.g., spectrophotometer) required. The capabilities of the system are validated *in operando* via i) photolysis tests of 12 water-soluble organic dyes to investigate the photostability under simulated sunlight; and ii) photocatalytic degradation of the four most photostable dyes – methylene orange, tartrazine 85, rhodamine B and direct black 38 identified from the photolysis results – using TiO_2 thin films prepared by atomic layer deposition. The applicability of the instrument is also demonstrated: i) using alternate photocatalysts – ZnO films and TiO_2 nano-powders; and ii) for the in situ detection of reactive oxygen species. The findings indicate that FaS-PhoReS exhibits consistent and repeatable results without being affected by factors such as i) non-uniformity of light intensity; ii) temperature and humidity; and iii) artefacts due to evaporation of the dye solution. Methylene orange and tartrazine 85 dyes are chosen to evaluate photocatalytic degradation, TiO_2 thin films annealed at 500 to 600 °C and TiO_2 nano-powders of 0.1 to 0.3 mg exhibiting better performance.

1. Introduction

An increasing concentration of water-borne pollutants is being reported in the environment. Examples of such micropollutants include pesticides, pharmaceutical compounds, and "forever chemicals" such as per- and polyfluoroalkyl substances.[1] Many of these micropollutants are not removed via traditional water treatment technologies, thus, there is an increasing demand for a sustainable treatment solution, which could enable effective removal at low energy consumption. One opportunity is solar-driven photocatalysis, based on materials that produce reactive oxygen species (ROS) when irradiated with sunlight. The ROS – such as hydroxyl radicals ($HO^{\bullet}$), singlet oxygen ($^1O_2$), and superoxide ($^{\bullet}O_2^-$) anions – can photodegrade water-borne pollutants, ideally achieving full mineralization.[2] Hundreds of possible organic and inorganic materials have been proposed for heterogeneous photocatalysis,[3] with perhaps a far greater number still waiting to be discovered. At the same time, 45 substances are currently listed in the European Union's Water Framework Directive as posing the greatest risk to the aquatic environment. The permutations and combinations of testing the effectiveness of all photocatalysts against all pollutants would require ≈10 000 experiments. This is before any other variables are considered – such as concentration of the pollutant, pH

E. M. Maloda, L. S. Daniel, D. Busko, A. Turshatov, J. S. Nyarige, B. S. Richards
Institute of Microstructure Technology (IMT)
Karlsruhe Institute of Technology (KIT)
Hermann-von-Helmholtz-Platz 1, 76344 Eggenstein-Leopoldshafen, Germany
E-mail: bryce.richards@kit.edu

The ORCID identification number(s) for the author(s) of this article can be found under https://doi.org/10.1002/admi.202401000

DOI: 10.1002/admi.202401000

E. M. Maloda
Department of Physics
Mathematics and Informatics
Dar es Salaam University College of Education
Box 2329, Dar es Salaam, Tanzania

L. S. Daniel
Multidisciplinary Research Services
University of Namibia
Private bag, Windhoek 13303, Namibia

B. S. Richards
Light Technology Institute (LTI)
Karlsruhe Institute of Technology (KIT)
Engesserstrasse 13, 76131 Karlsruhe, Germany

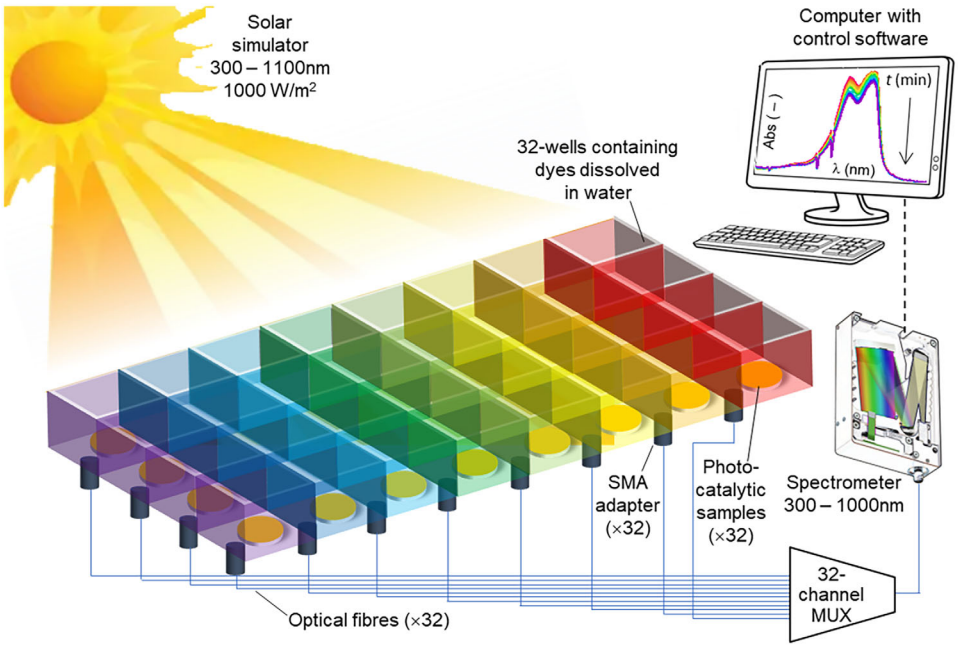

Figure 1. Overview of the fast-screening photocatalytic reactor system (FaS-PhoReS): an air-mass 1.5 global (AM1.5G) solar simulator illuminates the 32-well tray. In the case of photolysis experiments, each well contains a range of 12 dyes dissolved in water, whereas for photocatalysis experiments, an additional photocatalyst is placed on the floor of the well. A fraction of the sunlight transmitted through the liquid is coupled into the optical fibre screwed into the floor of the chamber. These 32 fibers are then connected to a 32-channel multiplexer (MUX) with one output channel connected to a spectrometer for the measurement of the transmitted wavelengths of light. A computer running Lab-VIEW software automates switching between channels and collecting spectra such that, over time, any photodegradation (evidenced as bleaching of the dye absorption) due to either photolysis and/or photocatalysis can be determined.

of the aqueous environment, temperature, as well as the spectrum and intensity of the light source, let alone combinations of materials, whether via heterojunctions or composites, which would massively increase the number of experiments. Thus, an *in operando* high-throughput fast-screening system would be extremely valuable in achieving accelerated evaluation and optimisation of such systems.

Typically, most researchers in the field of photocatalysis have employed various batch reactor systems to screen and study the properties of novel photocatalysts.[4] Subsequently, ultraviolet-visible (UV–vis) spectrophotometric measurements are used to evaluate the extent of photodegradation by measuring the changes in dye absorbance curves (the dye is considered as a model pollutant) as a function of time (typically hours) after exposure to a light source.[5] For example, researchers have employed separate instruments such as UV–vis spectrophotometric techniques, high-performance liquid chromatography (HPLC), and fluorescence imaging to evaluate the extent of photocatalytic activity.[5a,b,d,6] The serialized nature of such experiments –, that is, initially, the pollutants are photodegraded under a dedicated light source and then the degree of degradation is subsequently measured using external characterisation techniques – makes this approach slow and cumbersome. A more elegant solution that enables both in operando photodegradation and characterisation is illustrated in **Figure 1** and will be presented in more detail later.

Over the decades, combinatorial synthesis and high-throughput (HT) screening techniques have been extensively employed in drug development to generate novel antibodies from diverse molecular libraries.[7] Recently, several studies have reported the use of HT methods for screening materials.[8] For example, Xiang et al.,[8e,9] applied HT screening to evaluate 128 solid-state material libraries. This prompted researchers to employ HT photocatalytic screening approaches, to eliminate single sample measurements and to permit multiple samples to provide large amounts of high-quality data for machine learning algorithms.

Several studies have focused on assessing novel photocatalysts through HT techniques,[5a,10] and an overview of these is presented in **Table 1**. For example, Schmidt and co-workers employed different organic dyes to evaluate the photodegradation performance of TiO_2 nano-powders doped with transition and rare earth metals through photometric monitoring.[10b] The study of Ding et al.,[9] employed methylene blue (MB) as a probing pollutant to examine the efficacy of various novel photocatalysts under combinatorial synthesis. Yanagiyam et al.,[8d] constructed an elegant HT screening device for photocatalytic water purification using white-light emitting diodes (LEDs) at a low intensity of 1.65 W m^{-2}. The system allows the simultaneous testing of 132 photocatalytic reactions under consistent visible light exposure, temperature regulation, and stirring. One shortcoming of the system is the lack of integration of *in operando* optical characterisation –, that is, sample trays needed to be transferred to a microplate reader to measure the absorbance – thus limiting the effective throughput. Stöwe and co-workers investigated high-throughput screening investigations on metal oxide composites in a 60-fold parallel photoreactor using very high-intensity UV-LEDs (365 nm, 3840 W m^{-2}).[8a] Interestingly, the experiment

Table 1. Summary of HT screening systems for photocatalytic degradation of water-borne pollutants that have been investigated in the literature.

Goal of Screening+L9:S15	Light source	Photocatalyst	Operation condition	HT reactor type	Detection method	Batch size	Refs.
Assessment of novel photocatalyst nanoparticles for water purification	White-light LED	TiO_2, SnO_2, and WO_3 doped with 70 metals	in situ	Semi-automatic HT system with HPLC flasks	HPLC	45	[5a]
Evaluation of nanoparticles for photodecomposition of phenol	Fluorescent lamp	TiO_2 doped with Pt, Cu, Fe, Co, and Ni	in situ	HT photocatalytic reactor	UV–vis spectrophotometer	20	[5b]
Comparative study of nanoparticles for photodegradation of organic dyes	Xe lamp	TiO_2 – both undoped and doped with transition metals	in situ	HT analysis	Plates in UV–vis spectrophotometer	96	[18]
Investigation of novel photocatalysts of ternary oxides for water splitting	Xe lamp	ABO_3 (A = Y, La, Nd, Sm, Eu, Gd, Dy, Yb, and B = Al, In)	in situ	Combinatorial technique	Gas chromatograph	16	[9]
Investigation of photocatalytic thin films for H_2 production from water	Xe lamp	$Zn_{1-x}Co_xO$	in situ	Photoelectrochemical technique	Spectrometer	120	[19]
Evaluation of photocatalytic materials for water purification	White- light LED	TiO_2, ZnO and α-Fe_2O_3	*in operando*	HT reactor module	Microplate reader	132	[8d]
Discovery of photocatalyst thin films for water splitting	White-light LED	Co-doped TiO_2 films	in situ	2D pH imaging	pH	9	[20]
Discovery of heterogeneous catalysts for H_2 production	UV-A & vis-LEDs	C-doped TiO_2, bismuth oxides and other ternary oxides	in situ	HT instrument	Gas chromatograph	50	[21]
Examining the photoactivity of catalyst composites	Hg lamp	TiO_2, Nb_2O_5, WO_3, ZrO_2	in situ	Fluorescence photo-imaging	1,6-hexamethyl-enediamine probe	12	[22]
Conversion of pharmaceutical contaminants in water	UV-LED	TiO_2	*in operando*	Fluorescence imaging & HPLC	UV–vis spectrophotometer	96	[10e]
Multicomponent photocatalysts for the decomposition of organic pollutants	UV-LED	Cd, Ni, Zn, Sr, Ce, Y doped to MoS_2	in situ	Fluorescence Imaging	Spectrofluorometer	8	[23]
Evaluation of photocatalysts for water purification	UV-LED	TiO_2 and ZnO	in situ	Microplate photoreactor wells	UV–vis spectrophotometer	96	[24]
Assessment of photocatalytic activity of photocatalyst for water treatment	UV-LED	Various forms of TiO_2	*in operando*	Microplate reactor wells	Spectrofluorometer	96	[25]
Optimisation of colloidal water oxidation catalysts	Overhead	Metal oxide colloids of IrO_2 doped with Pt, Ru, and Os	in situ	Optical screening (96-well plates)	Bio-assay	96	[26]
Evaluation of composite photocatalysts for pollutant photodegradation	projector	$StTiO_2$ incl. composites w. WO_3, Bi_2O_3, CeO_2, g-C_3N_4, ZnO	in situ	Parallel photoreactor	plate reader	60	[8a]

focused on the degradation of the endocrine-disrupting compound 17α-ethinyl estradiol, however, the determination of photocatalytic performance relied upon ultrahigh performance liquid chromatography with tandem mass spectrometry coupling (UHPLC-MS/MS), which is not a technique that can be implemented in situ or *in operando*. Other works have focused on the development of in situ and *in operando* spectroscopies for photocatalytic studies. For example, both Hamoud et al.,[11] and Coronado et al.,[12] evaluated infrared, Raman, and X-ray absorption spectroscopies to understand what mechanisms are taking place and over what timeframes to improve photocatalyst design. However, in both cases, the potential of integrating such techniques into an HT screening system was not examined. Peter et al.,[13] reported the screening of five different compounds – methyl orange (MO), MB, phenol, salicylic acid, and rhodamine B (RhB) – using silver/TiO_2-SiO_2 nanocomposites under a mercury arc lamp (150 W) producing UV light in the range of 350 – 400 nm. In particular, the higher degradation rate of MB is due to photocatalysis rather than photolysis.

Most of the reported screening reactors employ UV-light sources. Relatively few works have used sunlight – for which the terrestrial standard is the air-mass 1.5 global (AM1.5G) terrestrial solar spectrum – that contains the full spectrum, extending from the UV out through the visible and into the near-infrared (NIR) region. The limited flux of UV sunlight of $1.51 - 2.01 \times 10^{21}$ photons $s^{-1}m^{-2}$ in the range of 300 – 400 nm wavelengths reaching the earth's surface is a big challenge to the wide range of photocatalysts. Subsequently, it is naturally more challenging than when relying on a narrow band of illumination that is specifically selected to match the region of weak absorption of the pollutant. Indeed, the International Standards Organisation (ISO) standard ISO: 10 678 for water purification using ceramic photocatalytic materials recommends using a UV-A range (320–400 nm) light source for investigating the photobleaching of a model pollutant (MB dye). This configuration is chosen as the MB dye absorption is weak in UV, while that of a photocatalyst such as titanium dioxide (TiO_2) is strong.[14] Thus, ISO: 10 678 is tightly defined around a specific photocatalyst–pollutant system. However, in reality, a wide range of pollutants and photocatalytic materials have their own unique optical properties and ability to generate a range of different ROS that can break selected chemical bonds, which will need to be employed. Thus, to further this sustainable

treatment technology that is driven by sunlight, it is vitally important to resolve the fraction of photodegradation that occurs due to either direct photolysis or photocatalysis.

The visible-light-driven assessment of novel photocatalysts with visible absorbing organic dyes has been identified by Ohtani and other research groups as being problematic due to self-sensitization,[15] for two reasons. First, this may lead to an incorrect photocatalytic activity, particularly when evaluating non-visible-light responding photocatalysts. Second, using maximum absorbance at a single wavelength was also highlighted as a problem for evaluating photocatalytic degradation.[16] Thus, the use of a UV–vis-NIR light source and broad absorption spectra of the organic dye in a wide range of wavelengths has been reported as the best approach for evaluating the photocatalytic activity.[15a,b,17] The present work builds on these guidelines using broadband simulated sunlight and integration of the entire absorption peaks for evaluation of true photodegradation.

To date, there have been no reports regarding a screening method that couples a reactor system with a fast detection method and automated software to control and facilitate data measurements and simultaneous recordings of multiple samples. In this work, a 32-channel HT fast-screening system – which will be referred to as FaS-PhoReS (fast-screening photocatalytic reactor system) – driven by simulated sunlight with *in operando* characterisation is presented. The system offers the following advantages: i) it is coupled with a UV–vis-NIR spectrometer and utilizes automated Lab-VIEW software to control and facilitate data measurements and simultaneous recordings. This allows for the continuous monitoring of the progress reaction, ii) eliminates the need to physically transfer the sample to the spectrophotometer, iii) is capable of processing 32 samples at once, which iv) minimizes labor and affords a time-saving process compared to existing techniques, v) utilizes a facile non-contact sensing technique based on optical fibers to detect light signals through the sample during the photodegradation process and vi) its vertical geometry for absorbance measurements alleviates any artefacts on measurement accuracy caused by evaporation. For evaluating the performance of the FaS-PhoReS, photolysis of 12 water-soluble dyes were evaluated, with the most photostable ones being further investigated for HT photocatalysis. To examine the photocatalytic performance of FaS-PhoReS, TiO_2 thin films were deposited via atomic layer deposition (ALD) onto UV-transparent fused silica substrates. The degradation of the four most photostable dyes (out of the initial 12) was then investigated. Particular care was taken to first demonstrate that dye degradation via photolysis was negligible before proceeding to evaluate dye removal via photocatalysis. To ascertain the efficacy and potential of the FaS-PhoReS system, this paper addresses the following research questions; i) How can an HT fast-screening system be designed to reliably resolve the contribution of both photolysis and photocatalysis to the photodegradation of water-soluble organic dyes when illuminated using terrestrial sunlight? ii) Which water-soluble dyes can be used as a model pollutant for HT fast-screening and exhibit the greatest photostability when exposed to simulated sunlight? iii) Which of the ALD-deposited TiO_2 thin films annealed at various temperatures exhibits the highest removal efficiency when photodegrading the photostable dyes under simulated sunlight? iv) Can the FaS-PhoReS system enable HT screening of photocatalyst nano-particles (powders) suspended in the solution? V) Can the ROS type(s) generated also be determined *in operando* using the same HT system?

2. Experimental Section

2.1. Design Concept of FaS-PhoReS

When conceiving FaS-PhoReS, the key design criteria for a successful system were being able to: i) resolve between photolysis and photodegradation; ii) achieve a >30-fold gain in automated throughput compared to single-beaker experiments; and iii) ensure that the results obtained are repeatable and not affected by artefacts. The latter encompasses being independent of any variations in external parameters such as fluctuations in light intensity, scattering due to suspended particles of photocatalyst, variations in relative humidity and temperature, as well as variations in water level – for example, caused by evaporation during the experiment (several hours). The batch reactor system consists of an aluminium sample tray, plastic container, optical fibers, multiplexer, spectrometer and computer with Lab-VIEW software for controlling measurements. The custom-built aluminium sample tray (262 × 232 mm) originated from the grass-root technique drawing of the block diagrams using visio software (detailed design and drawings presented in Figures S3–S6, Supporting Information). The bottom side of the tray was punctured holes for screwing the optical fibers for the detection of signals. The holes were technically designed and aligned on the side-lines to avoid blocking the optical sensor by the sample. An illustration of the FaS-PhoReS appears in Figure 1, where the simulated sunlight strikes the 32-well sample tray containing different dyes dissolved into water, while several photographs are given in Figure S1, Supporting Information. Sensing is realized via optical fibers that are screwed into the bottom of the Al tray, thus probing transmitted light from above the 32 wells.

2.2. Climate Chamber and Solar Simulator

Initially, it was foreseen that accurate control of both ambient temperature (T_{amb}) and relative humidity (RH%) of the environment would be important. For this reason, the entire experiment was designed to be conducted inside a climate chamber (DM340-CS-R, ACS, Italy) that had a solar simulator based on a high-power double-ended metal halide (MH) lamp (1200 W, Osram, Germany) mounted on the roof of the chamber. Under full illumination, the T_{amb} and RH% could be varied from 15 – 80 ± 1 °C and 10 – 80 ± 3 – 5%, respectively, The MH lamp was selected due to its; i) good match to the AM1.5G terrestrial solar spectrum (IEC standard 60068-2-5)[27] as plotted in **Figure 2**; ii) significant UV component, which places a more severe test on dye photostability requirements; and iii) high power, which allowed uniform irradiance of 100 ± 5 mW cm^{-2} over the 32 wells The uniformity of light intensity over the 262 × 232 mm sample area is plotted in Figures S2a,b, Supporting Information, both in terms of solar irradiance and photon flux (Equation S1, Supporting Information), respectively. The solar irradiance in Figure S2a, Supporting Information was measured using a calibrated silicon solar irradiance sensor (Si-V-1.5TC-T, Ingenieurburo, Mencke & Tegtmeyer, Germany). Later in the work, a second solar simulator based on a light-emitting diode (LED) lamp

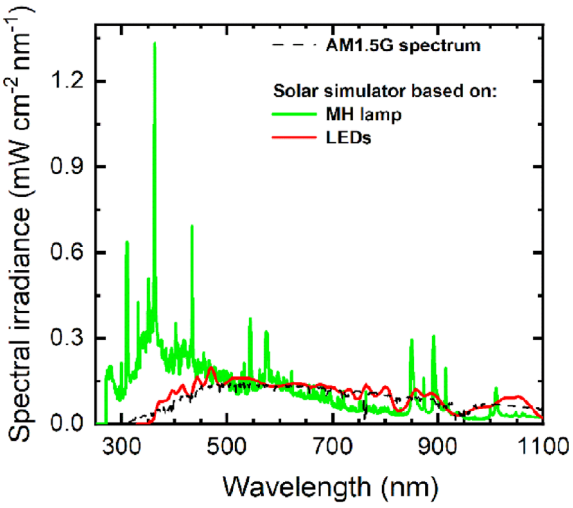

Figure 2. Spectral irradiance of AM1.5G terrestrial solar spectrum[27] compared to the two solar simulators used in this work – one based on a metal halide (MH) lamp and the other on a light-emitting diode (LED) lamp, the former being significantly richer in the UV/blue end of the spectrum.

(Sunbrick G2V.12.1.0, 0xD5249239, 9703–45 Avenue Edmonton, AB T6E 5V8) was evaluated. Although the spectrum exhibited a significantly smaller UV component, it matches the AM1.5G UV spectrum, which is much better than the MH lamp. The maximum illuminated area of this solar simulator is 260 × 260 mm, which closely matches the dimensions of the Al sample tray (detailed in Subsection **S1.2**). It emits an average of 100 mW $cm^{-2,}$ which was measured using a silicon solar irradiance sensor.

2.3. Sample Tray and Dyes

As mentioned in Section 2.1, the aluminium sample tray with UV-transparent borosilicate glass is comprised of a disposable polystyrene (PS) inner plastic container that holds the samples. The PS is comprised of a total of 36 wells, each measuring 32 × 30 × 36 mm internally (25 mL maximum volume), noting that only 32 wells are used in FaS-PhoReS (detailed below). Each well of the PS container is designed to accept a 25 mm-diameter sample, a size commonly used for photocatalytic membrane testing.[28]

For the initial validation of the applicability of the FaS-PhoReS, photolysis experiments were conducted on 12 selected water-soluble organic dyes at various concentrations to examine their photostability under simulated sunlight. These dyes include four cationic (positively charged) organic dyes-MB, RhB, indigotine blue (IB), and basic fuchsine (BF) – along with eight anionic (negatively charged) dyes; MO, uranine (U), alizarin reinst (AR), alizarin carmine (AC), nigrosine (N), terephthalic acid (TA), tartrazine 85 (T85), and direct black 38 (DB38). More information is provided in Table S1, Supporting information.

All dye chemicals were purchased from Kremer Pigments GmbH and Sigma Aldrich (Germany). The dyes were used as received without further modification. These dyes were selected based on their accessibility, affordability, potential photostability under sunlight, and solubility in water, as well as their frequent application in photocatalytic research. Additionally, they have relatively large extinction (photoabsorption) coefficients even at very low concentrations, facilitating absorption analysis using spectrophotometry.[29] Only the dyes that exhibited excellent photostability (minimal photodegradation) were chosen for evaluating photocatalytic performance. The three relatively low dye concentrations – 0.001, 0.01 and 0.1 mM – were selected based on the literature. The aqueous dye solutions were prepared by using one liter (1L) of deionized (DI) water (full details given in Subsection **S1.5**). In addition, the other family of water-borne pollutants as shown in Table S2, Supporting Information will be examined in the future.

2.4. TiO_2 Photocatalysts and Characterisation

TiO_2 was chosen because of; i) the UV component of sunlight results in the generation of $HO^{\bullet}$, one of the most powerful ROS; ii) good chemical stability and non-photo-corrosion when suspended in the aqueous solution, as well as iii) it is non-toxic and cost-effective.[30] Initially, TiO_2 thin films were utilized to explore the applicability of FaS-PhoReS to the photodegradation of various water-borne pollutants, motivated by previous work where TiO_2 photocatalytic membranes were successfully fabricated.[31] Two different substrates were used for TiO_2 thin film deposition; i) silicon (100) double-side-polished wafers with dimensions of 10 × 10 mm for materials characterisation only; and ii) fused silica glass substrates of 20 × 20 mm for optical characterisation and photocatalysis experiments. Further details on substrate preparation are provided in Subsection **S2.4.1** in Supporting Information. TiO_2 thin films were deposited onto both substrates using an ALD reactor (Picosun R-200, Finland) using titanium tetrachloride ($TiCl_4$, 99.999%, Sigma-Aldrich, Germany) and deionized water (H_2O) as sources of titanium and oxygen, respectively. The TiO_2 thin films were grown at 250 °C for 500 cycles at 4.5 h. The as-grown amorphous films were annealed in a Thermconcept furnace (KLS 05/13 2016, Fischer GmbH, Germany) from 300 – 750 °C in steps of 50 °C in the air for 1 h. Subsection **S2.4.2** (Supporting Information) provides more information regarding the ALD parameters.

The crystalline phase of the TiO_2 thin films was analyzed using X-ray diffraction (XRD, D2 Phaser, Bruker AXS GmbH, Germany) equipped with CuKα (λ = 1.54184 Å) radiation operated at a voltage of 30 kV and a current of 10 mA. The thickness of the films was measured using X-ray reflectometry (XRR, D8 Discovery, Bruker AXS GmbH, Germany), while the surface morphology and uniformity of the TiO_2 thin films deposited onto fused silica substrates were examined using a scanning electron microscope (SEM, Supra 60 VP, Zeiss, Germany). Optical absorbance spectra were measured using a UV–vis-NIR spectrophotometer (Agilent Cary 7000, USA) in two contexts; i) for comparative optical absorbance experiments (horizontal versus vertical geometries – see Subsection 3.2.3); and ii) to determine the optical bandgap of the TiO_2 films through Tauc plot analysis (Equations S2 and S3, Supporting Information). Additionally, TiO_2 nano-powders, 99.5% (Chempur: CAS No 13463-67-7, Fine Chemicals and Forschungsbedarf GmbH, Karlsruhe, Germany) with a particle size of 5 nm, were also employed in this study.

2.5. Optical Sensing

The glass floor of the sample container was ground to diffuse the light before it entered the optical fibre to; i) eliminate any sensitivity in the placement of the sample container; and ii) reduce the intensity of the transmitted optical signal, which often saturated the spectrometer. The 32 of the solarization-resistant 200 µm multimode optical fibers (M112L02, 0.22 NA, Thorlabs, Germany) enable UV–vis-NIR optical transmission data to be captured. These optical signals are sent to the key component in the system that enables HT – a 32-channel multiplexer (MUX, 32-MU 5 V, Weinert Fibre Optics GmbH, Germany). The USB-controlled optical switch connects all of the incoming 32 channels to be routed to the single output channel, which is connected to a single UV–vis-NIR mini-spectrometer (HDX01203, Ocean Insight, Germany) covering the 200 – 1000 nm wavelength range. Finally, a computer equipped with Lab-VIEW software reads out the optical data to monitor the degradation pathway.

2.6. FaS-PhoReS Experimental Protocol

The following experimental protocol was conducted using FaS-PhoReS for all dye degradation experiments – whether photolysis or photocatalysis. The climate chamber was set to a T_{amb} = 23 °C and RH = 40% controlled experimental conditions (Figure S1, Supporting Information). 20 mL of each dye solution, all with the same initial concentration, were accurately distributed into 30 wells of the PS containers, as illustrated in Figure S2, Supporting Information. Wells 31 and 32 were assigned to creating 0% and 100% transmission baseline values, that is, for the latter well 31 containing only water (no dye) monitored changes in the solar simulator´s intensity, while well 32 was blacked out. It should be noted that no stirring mechanism was involved during the irradiation. After 10 min in the dark, the lamp was switched ON, initiating photodegradation reactions. Throughout the degradation process, the intensity of transmitted light passing through the dye solution was recorded. For photolysis tests aimed to determine i) which of the 12 dye solutions was the most photostable and ii) at what concentration (0.001, 0.01, or 0.1 mM). The measurements were taken over a 120 min period, with transmission spectra recorded every 10 min in each well.

The four most photostable dyes (MO, T85, RhB and DB 38) from these photolysis tests were then selected for photocatalysis experiments at a concentration of 0.01 mM. A total of 22 ALDTiO_2 thin film samples onto fused silica substrates (2 × 2 cm) were distributed into 22 wells, with two additional wells designated for control experiments. The dye solutions of 20 mL in the wells were incubated for 12 h to achieve the adsorption of molecules on the active site of the photocatalysts. Photodegradation of mixed dye solutions with an initial concentration of 0.01 mM was also tested without and with TiO_2 films annealed at 600 ^{0}C. The mixed solution containing i) MO + T85, ii) MO + RhB, iii) T85 + RhB, each of 10 mL, and iv) MO + T85 + RhB, each of 6.5 mL, were distributed into the PS wells. Similarly, a photocatalytic degradation experiment using zinc oxide (ZnO) films coated-fused silica by the molecular precursor method (MPM) was also demonstrated. During the photocatalysis, transmitted signals were recorded at 20 min intervals over a total duration of 360 min. After the experiment, photocatalyst samples were sonicated in ethanol and rinsed with DI water five times to ensure that any remaining dye molecules were removed. The samples were then dried at room temperature for 12 h before being used for the next experiment. To ensure the reusability of the samples, each experiment was repeated three times for one dye. Moreover, the photocatalytic degradation test in the dark was carried out for a period of 6 h using ALDTiO_2 thin films annealed at 600 °C into the 20 mL of dye aqueous solutions (MO, T85, RhB and DB38) in the well. The aim is to investigate the degradation efficiency via adsorption of dye molecules into the surface of TiO_2 in the dark. The photocatalytic efficiency was evaluated by UV–vis-NIR spectrophotometer (Agilent Cary 7000, USA) by measuring the absorbance of the aliquot sample (2 mL). The degree of photodegradation efficiency was determined by the integrated absorbance at the entire wavelength of the major absorption spectra for each dye. Moreover, FaS-PhoReS has demonstrated the use of TiO_2 nano-powders (99.5%, CAS No 13463-67-7, fine chemicals purchased from Chempur GmbH, Karlsruhe, Germany) for two runs without stirring of the solution (full detailed in Section 3.4.3). Furthermore, the reactive oxygen species (ROS) detection – hydroxyl (•OH) radical and superoxide ($^{\bullet}O_2^-$) anions were also studied with FaS-PhoReS using Coumarin (Cou), 99% and nitroblue tetrazorium (NBT), 99% purchased from Sigma Aldrich chemicals. The aim was to determine whether the setup system can probe the •OH radicals and $^{\bullet}O_2^-$ anions generated during the photocatalytic degradation of Cou and NBT, respectively. In addition, the FaS-PhoReS set-up experiment (Figure S7, Supporting Information) under solar simulated LED lamp (Sunbrick G2V.12.1.0, 0xD5249239, 9703 – 45 Avenue Edmonton, AB T6E 5V8) at uncontrolled experimental ambient conditions was also conducted (full details given in Subsection **S1.5.2**). In this study, all degradation data were analyzed using Equations S4 and S5, Supporting Information for absorbance and photodegradation (%), respectively. Further information about the photodegradation experimental protocol is provided in Section **S1.6**.

3. Results and Discussion

3.1. Proof-of-Principle Operation

To illustrate the performance of FaS-PhoReS, photodegradation was demonstrated in two wells, without and with a photocatalyst under identical experimental conditions. An equal volume of 20 mL of a 0.01 mM methyl orange (MO) solution was placed in both wells. The solar simulator (MH lamp) was triggered ON for 360 min and measurements were recorded at 20 min intervals in ambient conditions of 23 °C and RH of 40%. MO was chosen for demonstration because it is one of the most stable dyes based on the photolysis results in this study. The photodegradation performance was computed by integrated absorbance in the 330–580 nm broad absorption range of MO. **Figure 3** presents the degradation of MO dye as a function of time – both as photolysis (no photocatalyst, Figure 3a,b) and using ALDTiO_2 thin film (20.5 nm thickness) annealed at 600 °C (Figure 3c,d). The results clearly show a trend of photodegradation in the presence of a photocatalyst and no significant change under the photolysis process. In addition, the TiO_2 photocatalytic test in the dark was conducted for 6 h, as presented in **subsection S1.6.1**. The

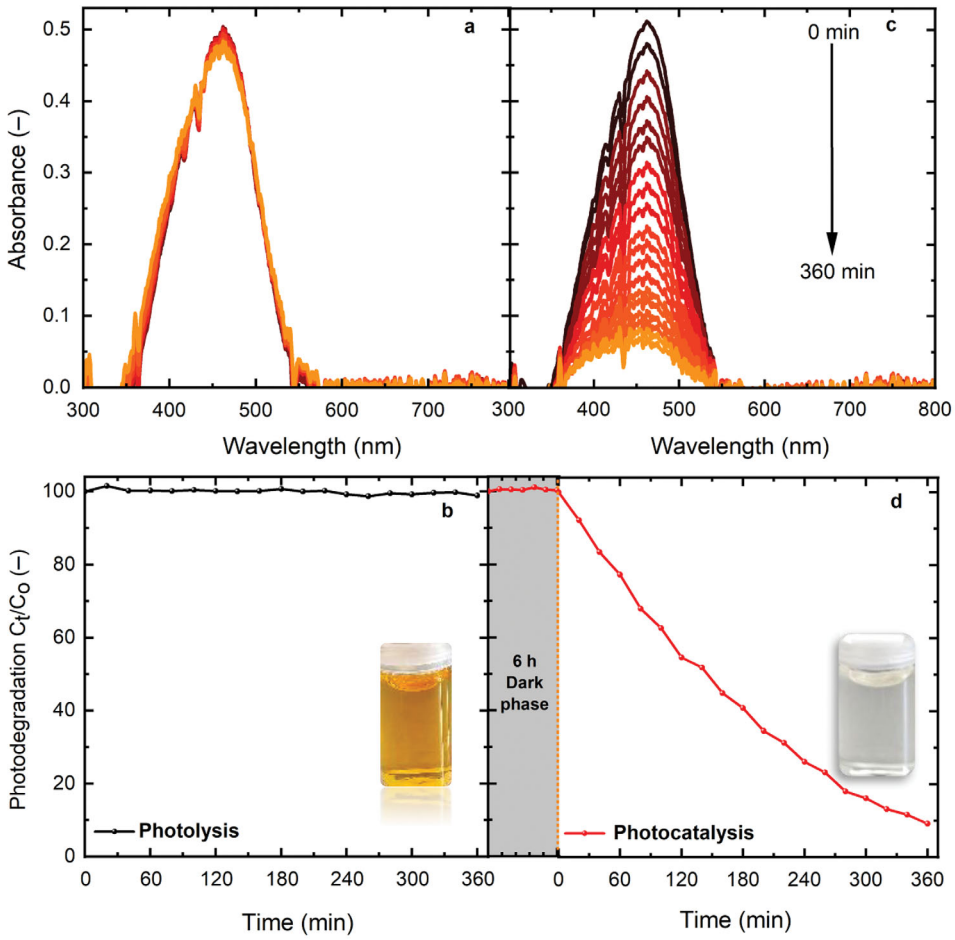

Figure 3. Time evolution spectral change and photodegradation of 20 mL MO dye aqueous solution with an initial concentration of 0.01 mM after 360 min due to a,b) photolysis and c,d) photocatalysis in the dark and light on using ALD-TiO_2 thin film annealed at 600 °C. The inset photos demonstrate the large degree of photodegradation that is achieved by photocatalysis, whereas via photolysis, this was almost zero. Single-run measurement.

observation revealed almost no degradation efficiency after 6 h in the dark, indicating that degradation efficiency is only reached due to photocatalysis rather than the adsorption of dye molecules.

3.2. Robustness of FaS-PhoReS Measurements

To demonstrate the robustness of the FaS-PhoReS across all 32 wells, the light intensity uniformity, T_{amb} dependence, influence of RH%, and the effect of evaporation in dye solution were investigated. These demonstrations were conducted using MO dye, one of the most stable dyes in this study. The goal was to comprehend the impact of these artefacts on the strengths of FaS-PhoReS in studying the true photocatalytic activity during the photodegradation process and to prevent artefacts from adversely affecting the results.

3.2.1. Influence of Uniformity of Light Intensity

The distribution of the simulated solar irradiance over the sample tray (Figure S2a, Supporting Information) shows a minimum of 93 mW cm^{-2} across the upper and lower wells and a maximum of 106 mW cm^{-2} at the centre. The measurements were taken in the climatic chamber at T_{amb} = 23 °C and RH = 40%. To demonstrate that, the slight non-uniformity light intensity had a minimal effect on the results, the direct photolysis and photocatalysis experiment of MO dye at a 0.01 mM concentration was conducted. 20 mL of MO solution was distributed in 30 wells without photocatalysts and irradiated for 360 min. Similarly, 30 wells with 20 mL MO aqueous solution in the presence of ALDTiO_2 films annealed at 600 °C were also performed. Wells 31 (containing only water) and 32 (kept in the dark) served as references for monitoring light intensity. The key observation of these photolytic degradation results (see Figure S8a, Supporting Information) shows only a slight variation, with the lowest and highest average values across all the 30 wells during the 360 min period differing by just 1.0% (absolute), from 97.9 to 98.9%, respectively. Moreover, the minimal influence of light intensity variation is also supported by the integrated absorbance results of various dyes across the 30 wells during photolysis, as shown in Tables S3–S8, Supporting Information. Moreover, the photocatalysis results demonstrated that non-uniform light intensity had a minimal impact, as illustrated in Figure S8b, Supporting Information

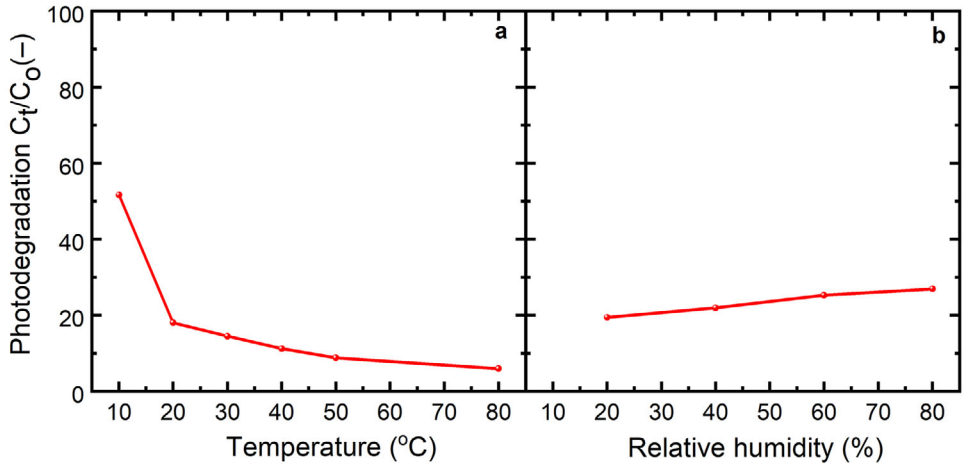

Figure 4. The influence of a) ambient temperatures ranging from 10 to 80 °C and b) relative humidity 20 to 80% on the photocatalytic degradation of 20 mL MO dye solution of an initial concentration of 0.01 mM for 360 min using ALD-TiO_2 thin films annealed at 600 °C in a single-run measurement.

of Supporting Information The observation revealed an average efficiency of 88 ± 6% due to spatial variation. The overall findings confirmed that the variation in light intensity distribution within the wells of the system had only a slight effect on the results.

3.2.2. Influence of Ambient Conditions

This section describes the impacts of a T_{amb} and RH during photodegradation experiments using the FaS-PhoReS. The demonstration was based on the T_{amb} and RH range of the climatic chamber when the solar simulator (setting of 55% of the light intensity, which is equivalent to one sun) was running. 20 mL MO photostable dye with an initial concentration of 0.01 mM was used alongside pristine anatase ALDTiO_2 thin films with a film thickness of 20.5 nm, annealed at 600 °C. The experiment was carried out over 360 min to evaluate the effects of these environmental conditions on the photodegradation process.

The influence of T_{amb} in the range of 10 to 80 °C at a constant RH of 40% on the photocatalytic degradation of MO dye solution is presented in **Figure 4a**. The temperature range was selected based on the T_{amb} limit settings of the climatic chamber in the presence of RH and simulated sunlight (see Table S9, Supporting Information). The results reveal a rapid increase in photodegradation from the temperature of 10 to 20 °C, followed by a more gradual increase from 20 to 80 °C. Photodegradation was minimal at 10 °C, intermediate between 20 and 40 °C and very high at 50 and 80 °C. In addition, significant evaporation of the dye solution was observed with an initial 20 mL volume reducing to 15, 13, 11, 9, and 8 mL at temperatures of 10, 20, 30, 40, and 50 °C, respectively. At 80 °C, evaporation increased dramatically, leaving only 1 mL. This result highlights the robustness of FaS-PhoReS to operate effectively within the 20 to 50 °C temperature range with a volume of 20 mL.

The low photocatalytic activity at 10 °C is attributed to an insufficient activation energy, which limits the adsorption of dye molecules and desorption of the degraded products from the TiO_2 surface, leaving the active sites for adsorption of other molecule dyes.[32] In contrast, temperatures ranging from 20 to 80 °C significantly increased photodegradation efficiency. The increase in temperature enhances the mass transfer rate, leading to high diffusion and mobility adsorption of MO molecules and desorption of final products from the surface of the photocatalyst.[29] The equilibrium between adsorption-desorption ensures that the active sites on the surface of photocatalysts remain available, allowing continuous adsorption of MO molecules. Therefore, an increase within this optimum temperature range likely promotes greater interaction between dye molecules and the photocatalysts. This observation agrees with the reported optimal range of 20 to 80 °C for photocatalytic performance.[33]

Figure 4b illustrates the effect of varying RH levels (20, 40, 60, and 80%) on the photocatalytic degradation of MO dye at a constant temperature of 23 °C. The results show a slight decrease in degradation from 85 to 75% as RH increases from 20 to 80%. The increase in RH promotes the increase in adsorption of water molecules on the surface of TiO_2, which blocks numerous vacant adsorption sites on the adsorbent to adsorb MO dye molecules.[32b,34] This competitive adsorption between the water and MO molecules onto the absorptive sites of the TiO_2 at high humidity weakens the photodegradation efficiency.[35]

3.2.3. Influence of Evaporation

As noted in Section 2.2.2, significant amounts of evaporation occur at various temperatures, influenced by the temperature and convection level in the laboratory environment. Normally, when water evaporation occurs in a cuvette, the absorbance measured using a UV–vis spectrophotometer will be higher over time as the dye concentration becomes greater. This scenario represents the "horizontal geometry" of absorbance measurement, where light passes through the cuvette (or well) of fixed dimensions as illustrated in **Figure 5a**. In contrast, FaS-PhoReS employs a 'vertical geometry' for absorbance measurements (**Figure 5c,d**), offering an elegant solution that mitigates the impact of evaporation on measurement accuracy. While evaporation still occurs and increases the dye concentration, it simultaneously reduces the optical path length through the dye solution layer. As a

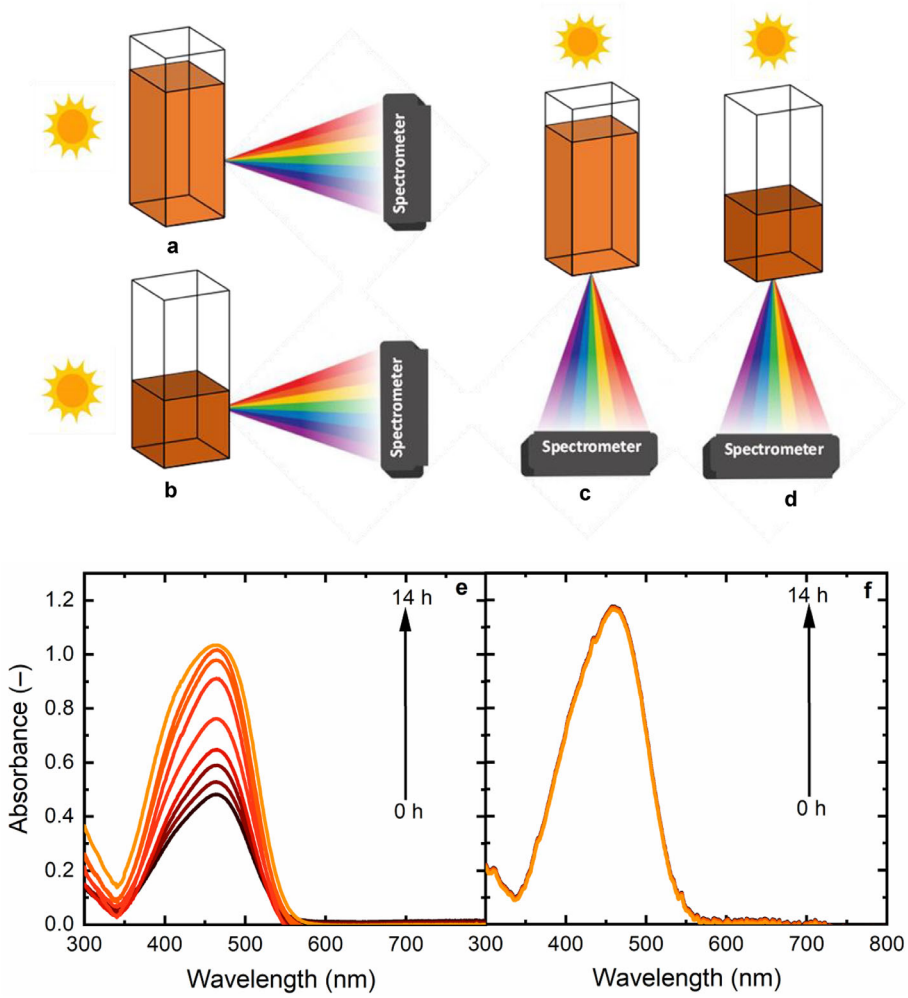

Figure 5. Large artefacts during the optical absorbance measurements can result due to evaporation, depending on the geometry of illumination. The horizontal illumination of a dye solution in a cuvette (e.g., measured using a classical UV–vis-NIR spectrophotometer) is shown at a) time zero and b) several hours later. The vertical illumination achieved via the FaS-PhoReS of a dye solution in a well is shown at c) zero time and d) several hours later. To quantify these illustrations, the absorption spectra MO (0.01 mM) dye solution measured over a 14 h period under AM1.5G simulated sunlight from the MH lamp is plotted using e) a cuvette in a conventional UV–vis-NIR spectrophotometer and f) and the well of the sample tray in the FaS-PhoReS, respectively.

result, the overall number of dye molecules remains unchanged. This means that the absorbance (optical density) measured using FaS-PhoReS in the vertical geometry remains accurate provided that enough water remains to keep the dyes dissolved.

The influence of dye solution evaporation on these two geometries was demonstrated using 0.01 mM MO solution in the beaker under a photolysis approach with the FaS-PhoReS illuminated by an MH lamp in the climatic chamber. After 14 h, the volume of the MO solution in the beaker was decreased from 40 mL to 10 mL. An aliquot of 2 mL of MO was collected in the cuvette at 2 h intervals and measured using a UV–vis-NIR spectrophotometer. The absorption spectra of the MO dye solution plotted in **Figure** 5e,f, as a function of irradiation time, were measured using i) the conventional horizontal geometry of a UV–vis-NIR spectrophotometer and ii) the vertical geometry of FaS-PhoReS, respectively. The result demonstrates that the UV–vis-NIR spectrophotometer showed a significant increase in absorption spectra (Figure 5e) due to changes in dye molecule concentration during evaporation. In contrast, the absorption spectra measured using FaS-PhoReS (Figure 5f) remain unchanged despite the dye molecules increasing in concentration over time, resulting from evaporation. This is attributed to the fact that the reduction in the optical path length in the vertical geometry is linearly proportional to the increase in the dye molecule concentration. This outcome underscores how the unique system design of FaS-PhoReS effectively prevents artefacts associated with evaporation from affecting the results.

3.2.4. Influence of Solar Simulator Spectrum

As illustrated in Section 2.2.3, significant effort was dedicated to employing a solar simulator with significant UV components, along with controlling the T_{amb} and RH%. To test whether these

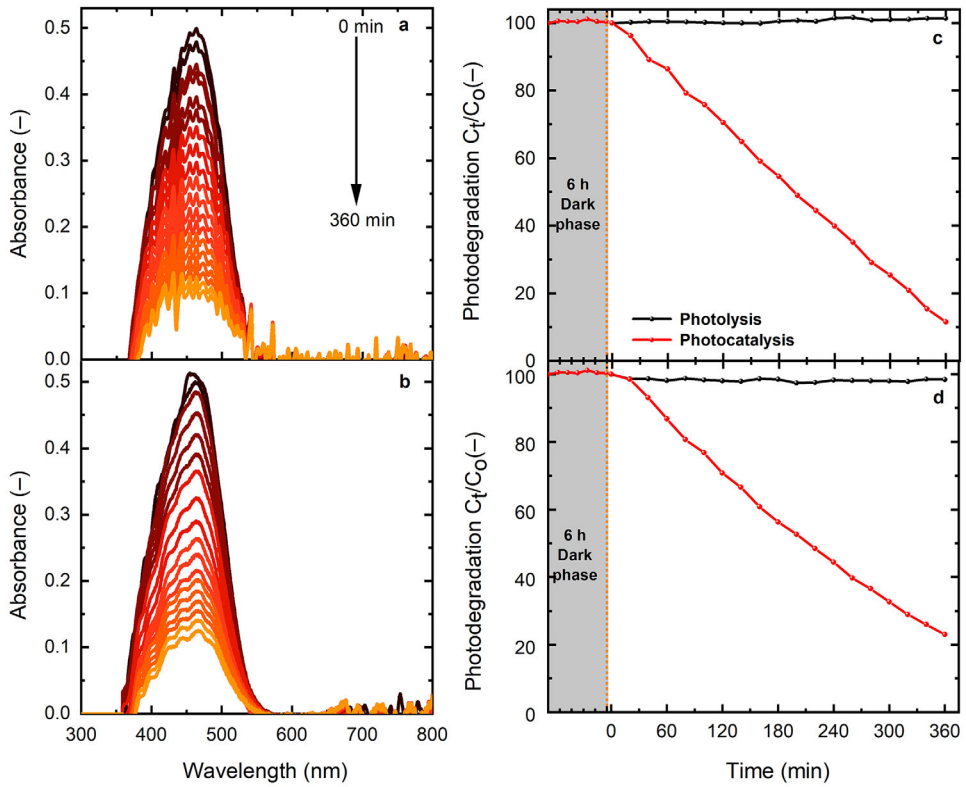

Figure 6. The photocatalysis of 20 mL MO (0.01 mM) dye solution after 360 min using two different solar simulators under FaS-PhoReS: MH lamp (top row) and LED-SolSim (bottom row) – plotted as a,b) time-dependent spectra and c,d) the degree of photocatalytic degradation in the dark and the presence of light with ALD-TiO_2 films annealed at 600 °C in a single-run measurement.

were needed, a FaS-PhoReS system using a solar simulator based on an LED lamp in the environment with no T_{amb} and RH% control was evaluated. The output spectrum of LED is plotted in **Figure** 2, where the amount of UV light is only 3.2 mW cm^{-2} (very similar to AM 1.5G UV content) compared to the 32 mW cm^{-2} supplied by the MH lamp in the climatic chamber – noting that both systems have an overall light intensity of 100 mW cm^{-2}. An experiment was performed to investigate the photocatalytic degradation subjected to these two solar simulators illuminating FaS-PhoReS for 360 min. The 20 mL of 0.01 mM MO dye solution with an ALD-TiO_2 thin film (annealed at 600 °C) were employed in both setups. The experimental details for LED-SolSim were presented in Subsection **S1.5.2** of Supporting Information.

Figure 6a,b describe the decrease in absorption spectrum curves due to photocatalysis, while Figure 6c,d illustrate photodegradation– representing an integration of each entire spectrum – after 360 min of the irradiation using the MH lamp (Figure 6a,c) and the LED-SolSim (Figure 6b,d). The spectral absorption shapes from the two sources are similar because an equal volume of 20 mL MO dye solutions was used during the study. The results reveal negligible photodegradation under direct photolysis for both sources of light energy. The high photocatalytic degradation of 90% was observed using an MH lamp while the volume was reduced to 14 mL. In contrast, the LED-SolSim achieved the removal of 79%, and the dye solution decreased to 18 mL. The significant reduction in volume is attributed to the evaporation due to the huge amount of UV light in the MH lamp compared to LED-SolSim. This also explains the dissimilarities of the photocatalytic performance between the two different sources of light. In addition, the achievement performance is also ascribed to the dissimilar experimental conditions, such as humidity and temperature control in the respective setup. Furthermore, the photocatalytic dark experiment was carried out for 6 h, as illustrated in **subsection S1.6.1**. The results reveal almost no change over 6 h. This suggests that degradation efficiency is only due to photocatalysis instead of adsorption. However, the findings reveal that FaS-PhoReS performed almost well in both experimental setup environments. This shows that the system can work at any source of light with sufficient energy for the photodegradation provided the coverage area of the tray sample. Thus, controlling the T_{amb} and RH% are not important parameters given the unique geometry of the Fas-PhoReS measurement.

3.3. Photostability Screening of 12 Organic Dyes under Simulated Sunlight

The FaS-PhoReS under the climatic chamber (MH lamp) was employed to examine the photolytic properties of six different water-soluble dyes that have been applied in the literature as model water-borne pollutants; namely methylene blue (MB), rhodamine B (RhB), tartrazine 85 (T85), methyl orange (MO), terephthalic acid (TA) and direct black 38 (DB38) and the addition of six other

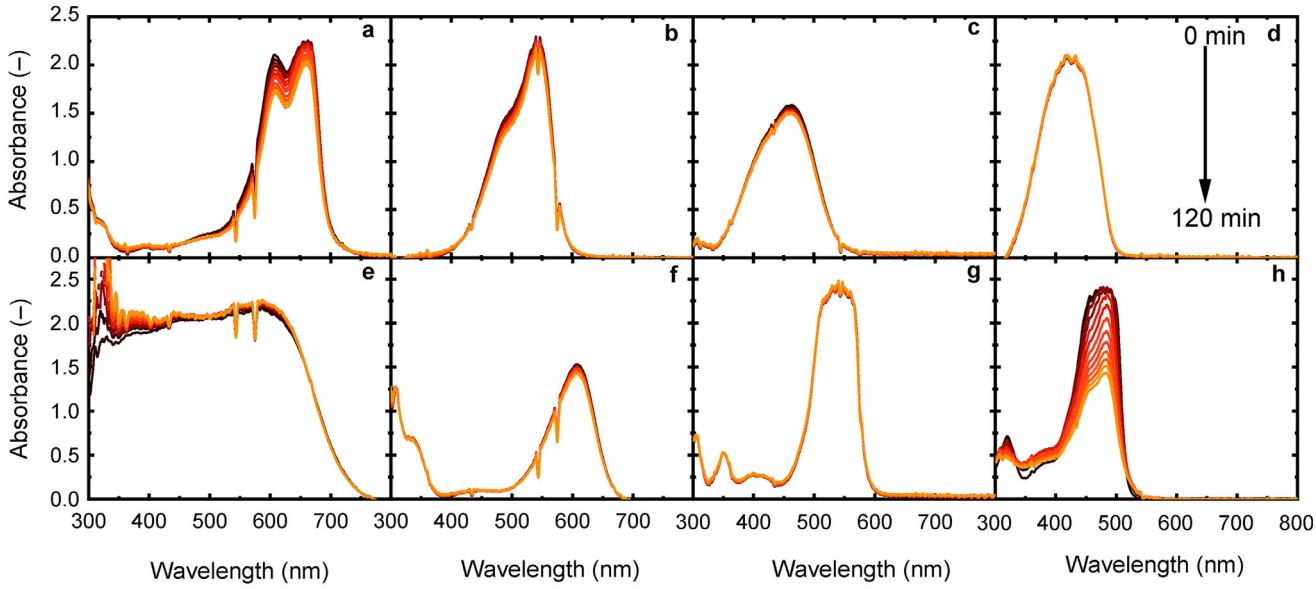

Figure 7. The photolysis time-dependent absorption spectra of eight strong absorbing dyes (each of 20 mL into the well) at a concentration of 0.1 mM over a period of 120 min undergoing photolysis under simulated air-mass 1.5 global (AM1.5G) sunlight (MH lamp of FaS-PhoReS system): a) methylene blue (MB) b) basic fuchsine (BF) c) methylene orange (MO) d) tartrazine 85 (T85) e) direct black 38 (DB38) f) indigotine blue (IB) g) rhodamine B (RhB) h) uranine (U). The presented absorption spectra results are from one well among the five wells containing each dye solution for single-run measurement.

new dyes namely indigotine blue (IB), basic fuchsine (BF), uranine (U), alizarine reinst (AR), alizarin carmine (AC), nigrosine (N). The goal was to investigate and identify the dye(s) with suitable absorbance at low concentrations (0.001, 0.01, or 0.1 mM) and assess their photostability when exposed to a broad spectrum of simulated sunlight (100 mW cm^{-2}). The assessment was carried out for 120 min for the quick identification of the stable dyes before conducting further studies for a longer irradiation time. The measurements were taken for one run with five wells containing equal volumes of the same dye solution, and the average photodegradation was computed. It is important to note that the various intermediate products produced during the photodegradation pathway have been reported in the literature.[36] The photolytic characteristics of the dyes are contingent upon the chemical composition of the compounds, aromatic rings, and the ability of photon energy to penetrate the dye solution to dissociate water molecules to generate hydroxyl radicals, which promote photodegradation.[36]

Figure 7 illustrates the absorption spectra at 0.1 mM concentration of eight dyes that exhibit substantial absorption with a chemical structure presented in Table S1, Supporting Information. Four dyes – AR, AC, N, and TA – did not exhibit significant optical absorption even at the highest concentration of 0.1 mM (plotted in Figures S17–S20, Supporting Information) and were therefore not further investigated in this study. As indicated in Figure 7, the results reveal high absorption spectra for the concentration of 0.1 mM compared to 0.01 and 0.001 mM as presented in Figures S9–S16, Supporting Information. The difference in absorbance on the same dye is due to differences in dye molecules present in initial concentrations. Two dyes (MB and U) exhibit a significant decrease in absorption, four others (BF, IB, RhB, BD38) display a slight change, while two of them (MO and T85) exhibit almost no change after 120 min of exposure. The difference in absorption bands depends on the amount of photon penetration into the dye solution due to the dissimilar aromatic rings of the chromophore group of each dye.[37] The high disappearance in absorption bands of MB and U is due to dye molecules absorbing more photons. However, MO and T85 possibly absorb the photons, they could not be degraded probably due to insufficient energy of photons to break the bonds.

The average integration photodegradation of the eight strongly absorbing dyes at all three dye concentrations is depicted in **Figure 8** when exposed to simulated sunlight for 120 min. Note that the photodegradation performance was computed by integrated absorbance in the major absorption spectra of each dye. The observation indicates a significant decrease in photolytic degradation of the MB, U, BF and IB, while gradual for the MO, T85, RhB and DB38 with increasing initial dye concentration (see Table S10, Supporting Information). The low photodegradation in 0.1 mM is due to high optical density, suppressing the light penetration into the dye solution. In addition, the non-degradable dye molecules in 0.1 mM can be explained by less permeable photons compared to 0.01 and 0.001 mM concentrations. This is attributed to the amount of dye molecules present in the solution, which enhances the penetration of photons.[38] Note that the system can work with other water-soluble pollutants that exhibit absorption in the 300–1100 nm range due to the limitation of a wavelength range of light source.

The increase in degradation of MB, U, BF and IB dyes is probably ascribed to more photons absorbed by the dye molecules that enhance the high generation of •OH radicals, which have a high affinity with chromophore bonds.[39] This is due to the fact that •OH radicals oxidize the dye molecules into smaller molecules through photochemical reactions. *Joseph* et al.,[40] also reported

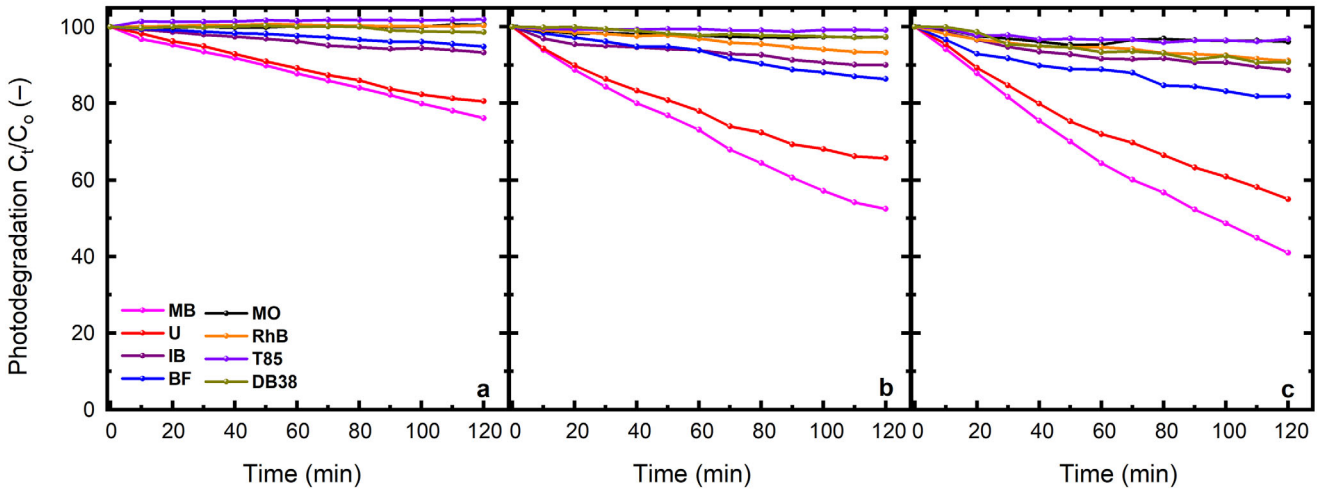

Figure 8. The photolysis average photodegradation of eight dyes (each of 20 mL into the well) with initial concentrations of a) 0.1 mM; b) 0.01 mM; and c) 0.001 mM after 120 min. The presented results are the average of five wells for single-run measurement.

high photolysis of MB in a water-based solution when exposed to ultraviolet lamps (UV-C, UV-B and UV-A) and a solar lamp, each with 10 mW cm^{-2}. In contrast, it is clear from Figure 8 (see also Table S10, Supporting Information) that photodegradation of MO, T85, RhB and DB38 dyes for three concentrations is significantly below 8% after 120 min, thus exhibiting excellent photostability. Further testing with these four dyes (MO, RhB, DB38 and T85) was conducted, exposing them for 15 h of simulated sunlight (as plotted in Figure S21, Supporting Information). Overall, the results here are consistent with what the literature, as discussed below – nothing that unfortunately only the lamp power is often reported and not the light intensity. DB38 was reported to be photolyzed up to 7.0% when exposed to a mercury vapour lamp (80 W).[6] Kader et al.,[41] observed a 5.3% degradation of MO after 5.5 h of exposure to five UV (20 W) lights. Similar observations under UV-C light at a wavelength of 245 nm were also reported by Boukhedou et al.,[42] and Bendjama et al.,[43] using a source of UV-C (15 mW cm^{-2}) at 254 nm. Guettai and Amar also documented 5.5% photolysis of MO when exposed to UV-lamps (2 × 15 W) after 5 h of irradiation.[44] Subsequently, the authors demonstrated non-photodegradable MO when exposed only to visible light. A similar trend of non-photolyzed MO under UV–vis light irradiation was observed after 9 h.[45] The study conducted by Bouarroudj et al.,[36] reported very low photodegradation of T85 under direct photolysis when it was exposed to UV lamps (18.6 W m^{-2}, 365 nm) and sunlight (853 W m^{-2}) after 90 min of irradiation. The group of Utami et al.,[46] demonstrated that RhB did not degrade when subjected to visible light but was vulnerable to photolysis under UV light (8 W) at an irradiation time of 90 min. In addition, the negligible removal of RhB was witnessed by the study of Alakhras et al.,[47] using UV light after 80 min and Alle et al.,[48] with UV-A lamps (14 W m^{-2}, 365 nm) for 120 min. Furthermore, Guimaraes et al.,[49] demonstrated removing 2% of Rh-19 exposed to UV light (65 W, 254 nm) after 5 h.

This study demonstrated that a high concentration of 0.1 mM (high absorption) promotes retardation of degradation due to limited penetration of photons into the solution as reported by Bouarroudj et al.[36] This observation agrees with the work reported by Soltani and Entezari,[50] and the work of Bendjabeur et al.,[51] The concentration of 0.01 mM revealed an intermediate absorbance and photodegradation due to a little dye molecules that do not intercept the depth of the photons to penetrate. Thus, the primary concentration of 0.01 mM was selected as an ideal for photocatalytic investigations in the FaS-PhoReS. This is the same concentration specified by the International Standards Organization (ISO) (ISO-10678) for MB and is considered the most acceptable for such purposes,[14] Moreover, the study revealed that MB, U, BF and IB are highly photolyzed whereas RhB and DB38 exhibit minimal photolysis, with MO and T85 demonstrating exceptional photostability. These results suggest that the low degree of photodegradation observed in MO, RhB, DB38 and T85 under photolysis makes them ideal candidates for investigating the photocatalytic degradation of the novel photocatalysts in a broad range of the spectrum. This is because most of the photons can penetrate the depth of the dye solution to reach the active sites of the photocatalyst with insignificant photosensitization. This addresses the challenges associated with using organic dyes in the visible light range as highlighted by Ohtani et al.,[15a] and, thus, clears the path for the further development of solar-driven photocatalytic technologies.

3.4. HT Photocatalytic Screening of Four Photostable Dyes under Simulated Sunlight

3.4.1. Structural, Morphological and Optical Properties of ALD TiO_2 Thin Films

Before detailing the photocatalytic results, it is first necessary to briefly describe the structural, morphological and optical properties of the ALD-deposited photocatalytic TiO_2 thin films (more detailed information on deposition can be found in Subsection S2.4.2 of Supporting Information). The XRD patterns of all samples – the uncoated silicon and fused silica substrate, as well as the as-deposited and annealed TiO_2 thin films – are presented in

Figure S28, Supporting Information. The absence of any peaks in the as-deposited films indicates that it is in an amorphous phase, which agrees with previous studies using thermal ALD.[52] This is in contrast to the findings for plasma-enhanced ALD TiO_2 films, where Lee et al.,[53] as well as Cheng and Chen [88], already observed the anatase structure at deposition temperatures of 250 °C. The TiO_2 films deposited onto both substrates and annealed at temperatures ranging from 300 to 750 °C were polycrystalline, exhibiting the main anatase (101), while the (004) and (200) peaks were not observed. A slight increase in the intensity of the main peak (101) was noted for the TiO_2 films deposited onto silicon with increasing annealing temperatures from 300 to 750 °C, as plotted in Figure S28a, Supporting Information, which suggests a slight enhancement in the degree of film crystallinity with temperature. The same increase was not observed for TiO_2 films deposited onto fused silica substrates (Figure S28b, Supporting Information), partially due to the large overlap with the background signal from the amorphous substrate. No evidence of the rutile phase was observed in any samples, even for samples annealed at 750 °C, which agrees with other reports. Hsu et al.,[54] reported a similar result with ALD TiO_2 annealed at temperatures ranging from 350 to 750 °C in nitrogen gas for 30 min. Moreover, Dang et al.,[55] also observed no phase transformation from anatase structure to rutile phase when the PE-ALD TiO_2 thin films were heated from 500 to 900 °C in the air for 1 h. The study of Pheamhom et al.,[56] similarly found no change in the anatase crystal structure of the ALD TiO_2 films at annealing temperatures ranging from 450 to 650 °C in the air for 1 h.

The SEM images (Figure S29, Supporting Information) indicate the surface morphologies of the TiO_2 thin films, both as-grown and annealed at temperatures of 300 to 700 °C. The images display a coarse and compact structure with small grains of crystallites covering the whole substrate surface, becoming more noticeable at 700 °C, likely due to increasing grain size. It is evident from the images that the coated films were homogeneous and uniformly distributed over the substrate with roughness and pinholes-free – such defects could limit the performance of photodegradation efficiency.[57]

Figure S30a,b, Supporting Information illustrates the optical absorption spectra and Tauc plot for determining the optical bandgap (E_g) of as-deposited and annealed TiO_2 thin films. The as-grown films exhibit a higher bandgap (E_g = 3.4 eV) and lower absorbance, both consistent with the formation of amorphous TiO_2.[55,58] Once annealed, the bandgap of all samples decreased (E_g = 3.2 – 3.35 eV) and the absorption strength increased, thus enhancing the amount of UV light being harvested. The bandgap change after annealing to lower values is attributed to the change in film density and grain size.[58] The bandgap values of the ALD TiO_2 here are similar to the findings of Lee et al.,[59] and slightly lower than the ~3.4 eV values reported by Badovinac et al.,[60] and Liu et al.,[61] There is no clear trend with temperature, a finding that has been observed in the literature before.[62] Table S11, Supporting Information illustrates the thicknesses of as-deposited TiO_2 films and annealed films in an ambient environment in a furnace at temperatures ranging from 300 to 750 °C in steps of 50 °C. The thicknesses were determined by X-ray reflectometry (XRR) analysis by fitting the fringe patterns of the measured sample curves with simulated fringes. The as-grown films on fused silica had a thickness of 26.4 nm, which corresponds to an ALD growth rate of 0.052 nm per cycle. As the annealing temperature increased, the thickness of the films decreased steadily – from 24.8 nm at 300 °C to 18.8 nm at 750 °C – revealing the expected film densification with increasing temperature. This is due to the transformation of the unsaturated defects of TiO_2 films into a high degree of crystallinity phase and then dimensional changes due to shrinkage, thus the decreases in thickness.

3.4.2. Photocatalytic Performance of ALD-TiO_2 Thin Films with Photostable Dyes using FaS-PhoReS

Building on the outcome of the photolysis experiments – that four of the investigated dyes exhibit excellent long-term photostability – a set of experiments was designed to investigate the photocatalytic performance of the ALD TiO_2 thin films (as-deposited at 250 °C and annealed from 300 to 750 °C) in degrading the selected dyes. Thus, the PS wells in FaS - PhoReS were filled with MO, RhB, T85, and DB38 dye aqueous solution, each with an initial concentration of 0.01 mM. Overall, the two dyes (MO and RhB) were each loaded into 12 different PS wells (24 wells used out of 30) and 6 wells were left due to the number of samples to be tested. For both dyes: i) two PS wells contained no photocatalysts for control experiments. This is to confirm that any photodegradation observed originates only from the excitation of photocatalysts rather than the self-photosensitization of dyes by visible light;[15a] while ii) the remaining twenty-two wells each had a 20 × 20 mm TiO_2 thin film (fused silica substrate) placed at the bottom. A similar fashion was repeated for T85 and DB38 dyes using the same TiO_2 films after being sonicated in ethanol and rinsed with deionized water five times before being dried at room temperature for 12 h. Each experiment was performed in triplicate for every dye to ensure the system´s data repeatability. A FaS-PhoReS experiment of 360 min duration was chosen to evaluate photocatalytic performance using simulated sunlight from the MH lamp.

Figure 9 summarizes the results for the one cationic dye (RhB) and three anionic dyes (MO, T85, and DB38) under direct photolysis (Figure 9a–d) and photocatalytic degradation using ALD-TiO_2 thin films annealed at 600 °C (Figure 9e–h). The temporal evolution of the absorption spectra indicates that no decrease could be measured for T85 (Figure 9a) and MO (Figure 9c), while a significant decrease was observed for RhB (Figure 9b) and DB38 (Figure 9d) under photolysis. Thus, it is recommended that T85 and MO dyes should be selected for any future photodegradation research using terrestrial sunlight. It is also potentially useful that one of these dyes is cationic (T85) while the other is anionic (MO), as will be discussed in more detail below. The photocatalysis results in Figure 9e–h indicate the gradual disappearance of the distinct absorption bands of each dye as a function of irradiation time for the 600 °C-annealed TiO_2 thin films. This indicates the significance of photocatalysts during photodegradation. The photocatalytic spectra of the remaining TiO_2 samples can be found in Figure S22a–j, Supporting Information. To provide an overview, the degree of photodegradation of the same four dyes is displayed in **Figure 10**, both with and without photocatalysts present, and now including the as-deposited TiO_2 sample (250 °C) as well as those annealed at all other temperatures (300 – 750 °C). At this point, it is important to note that the

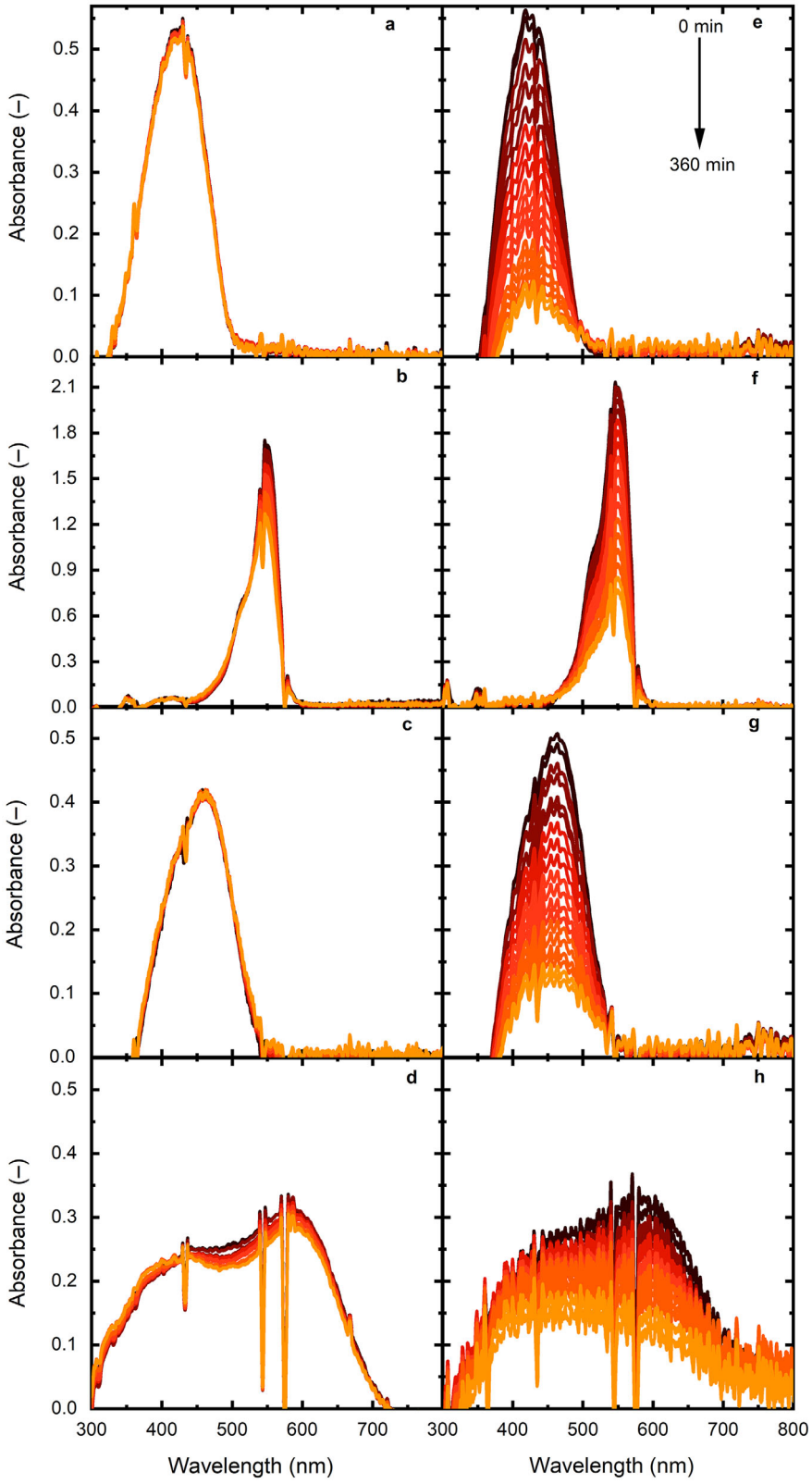

Figure 9. Photolysis a–d) for control experiment and ALD-TiO_2 (600 °C) photocatalysis e–h) temporal evolution absorption spectra of T85, RhB, MO and DB38 dyes (each of 20 mL in their respective wells) respectively at an initial concentration of 0.01 mM after 360 min.

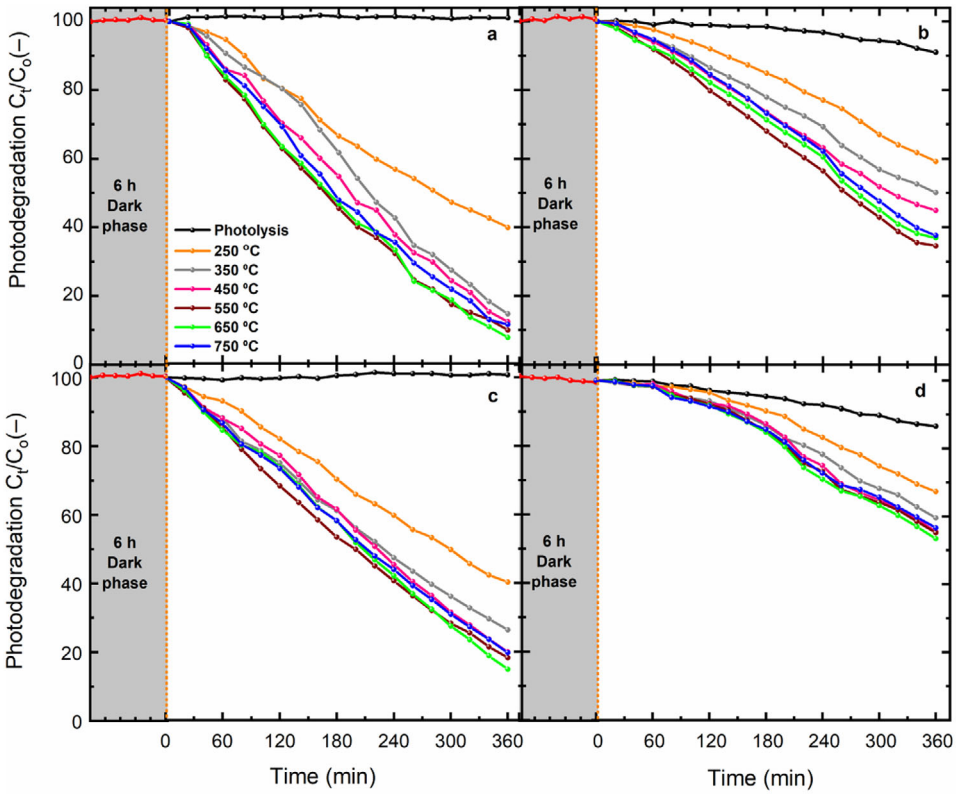

Figure 10. The photocatalytic performance of the removal of four dyes (each of 20 mL in their respective wells) with an initial concentration of 0.01 mM after 360 min in the dark (ALD-TiO_2 thin films annealed at 600 °C), as-deposited (250 °C) and annealed (350–750 °C) ALD-TiO_2 thin films in 20 mL of: a) T85; b) RhB; c) MO; and d) DB38. The results are the average of three repeat measurements with the same samples.

photodegradation performance was assessed using the integrated absorbance from the main absorption spectrum of each dye rather than just the maximum absorbance at a single wavelength (Table S12, Supporting Information), which is often the case in the literature. For instance in this work, the integrated absorbance of MO is calculated in the 330–580 nm broad range of the absorption band while T85, RhB and DB38 are in the 320–510, 470–600, and 400–700 nm range, respectively. The integrated absorbance approach helps to avoid the potential for self-photosensitization of dyes in the visible light range, which could otherwise lead to misleading photocatalytic activity results, as highlighted by Ohtani et al.,[15a] and Amalia et al.[16b] Similarly, it saves the challenge of spectra shift (red-shift or blue-shift) during the photodegradation reaction, making it problematic for accurately evaluating photodegradation efficiency from the absorbance of the characteristic peak.

From Figure 10, it can be seen that the degree of photodegradation in the dark is almost zero after 6 h for all dyes, while due to photolysis alone is close to zero for MO and T85, while RhB and DB85 exhibit ≈9 and 12% removal, respectively. The dark experiment demonstrated that photodegradation efficiency is attributed to the presence of sufficient energy that exhibits adsorption-desorption equilibrium on the active sites of the TiO_2 surface. The photocatalytic results reveal the higher degradation for MO and T85 dyes, while lower for RhB and DB38 for all TiO_2 thin films regardless of the different annealing temperatures. From the results, the as-deposited (250 ^{0}) TiO_2 films exhibited minimal removal of 61, 40, 59 and 33% for T85, RhB, MO, and DB38, respectively. This is due to the high degree of TiO_2 amorphous phase, which promotes the trapping of electron-hole charge carriers.[63] In addition, the amorphous phase generates poor charge carrier conduction because of the broad bandgap energy. In contrast, the films annealed at 300 (Figure S23, Supporting Information) and 350 °C showed removal of 80 and 84% for T85, 45 and 47% for RhB, 68 and 74% for MO, 35 and 40% for DB38, respectively. The low photocatalytic degradation at low temperatures might be attributed to the high number of crystal defects due to the weak crystallinity phase.[57] The defects are detrimental to photocatalytic activity since they act as trap sites for the photogenerated charge carriers and promote recombination.[57] At higher annealing temperatures from 450 – 750 °C (see also 400 – 700 °C in Figure S23, Supporting Information), it is observed the increase in photocatalytic activity about 86 to 93% for T85, 50 to 66% for RhB, 80 to 85% for MO and 40 to 50% for DB38 for the films annealed at a temperatures ranging from 450 to 650 °C and slightly drop for 700 and 750 °C after 360 min. The increase in activity performance with increasing annealing temperatures is attributed to the phase transition of amorphous TiO_2 to the suitable formation of the polycrystalline (nanocrystalline) anatase phase with a rough surface, which is the key feature for the photocatalytic degradation.[57,63,64] In addition, anatase TiO_2 has a higher charge carrier lifetime and more negative conduction band edge for the suitability of the photo-generated electrons to reduce molecular oxygen to reactive

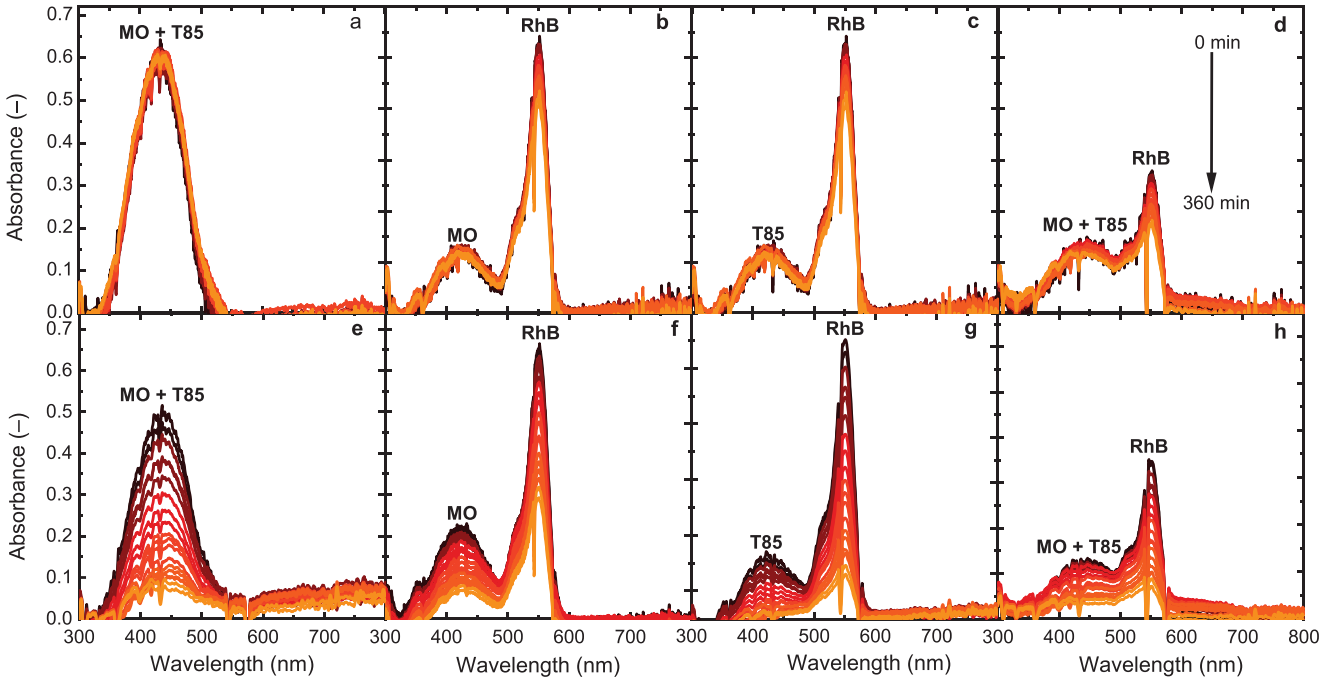

Figure 11. The temporal variation of absorption spectra of the mixed dye solution of MO + T85, MO + RhB, T85 + RhB (1:1 volume ratios) and MO + T85 + RhB (1:1:1 volume ratios) with an initial concentration of 0.01 mM after 360 min due to a–d) photolysis and e–h) photocatalysis using TiO_2 films annealed at 600 °C, respectively.

oxygen species, which are strong enough to degrade micro-organic pollutants in water.[63,65] The higher removal of T85 anionic dye is ascribed to the high diffusion rate of dehydrated dye molecules to active sites of the TiO_2 and due to direct bonding of the sulfonic group, which enhances the adsorption of dye molecules onto the active sites of TiO_2. However, the limited levels of low photodegradation observed in cationic RhB are possibly due to the low rate of diffusion of hydrated molecules to reach the surface of the TiO_2.[66] Further the result reveals a high photodegradation efficiency of the negatively charged MO anionic dye, despite the repulsive from the surface charge of TiO_2. This could be explained by the acidity-basicity behavior of the dye solution due to sulfonic group, which probably reduces the electrostatic repulsion between the like charges. This property promotes a more intense and efficient redox reaction of the dehydrated molecules with reducing-oxidizing agents generated due to the excitation of TiO_2 by photons. Instead, the low degradation on negatively charged DB38 is attributed to repulsive with negative charges of the TiO_2 and hydrated dye molecules. Additionally, DB38 probably absorbs a lot of photons and thus, few of them reach the active sites of the TiO_2.[67] This leads to a reduction in the number of photogenerated electrons and holes that might result in a decline in the effectiveness of photocatalysis.[68] These results demonstrate outstanding photocatalytic performance for the annealed TiO_2 from 400 to 650 °C compared to as-grown and annealed at 300 (Figure S23, Supporting Information) and 350 °C. In contrast, control experiments demonstrated the superior photostable dyes – MO and T85, which are non-degradable under photolysis. These dyes are greatly confirmed to be used to investigate the true photocatalytic activity of photocatalysts in a wide range of light intensity since most of the photons can reach the surface of photocatalysts without being absorbed by dye molecules.

Furthermore, to demonstrate the suitability of the system for the photodegradation of industrial wastewater consisting of multiple dye solutions, mixtures of MO + T85, MO + RhB, T85 + RhB and MO + T85 + RhB (with an initial concentration of 0.01 mM of each component) was demonstrated for a single run using ALDTiO_2 thin films annealed at 600 °C. The choice of dyes was based on whether they exhibited an overlap in the absorption spectra (MO + T85) or not (MO + RhB and T85 + RhB). **Figure 11** presents the full optical absorbance of mixed dye solutions due to photolysis (**a-d**) and photocatalytic TiO_2 films (**e-h**) after 360 min of irradiation with simulated sunlight (MH lamp). The MO + T85 dye mixture (Figure 11a,e) exhibits an absorption spectrum comprised of 330 – 560 nm (480 nm peak) and 320 – 510 nm (427 nm peak) for MO and T85, respectively. The solution of MO + RhB (Figure 11b,f) and T85 + RhB (Figure 11c,g) shows distinct absorption peaks due to dissimilar absorption wavelengths of RhB located in the 470 – 600 nm (534 nm peak) range. During photolysis (Figure 11a–d), MO and T85 demonstrated a negligible change in absorption spectra in all experiments, while a slight decrease in absorption was noted for RhB after an irradiation time of 360 min. In contrast, the photocatalytic TiO_2 results in Figure 11e–h show continuously decreased absorption bands of each dye component in mixed solutions as a function of irradiation time. This highly signifies the potential of FaS-PhoReS during degrading wastewater containing mixed dyes using photocatalysts.

To provide an overview of photodegradation performance, **Figure 12** presents the degree of degradation levels of four sets of mixed dye solutions in the absence and presence of TiO_2 films.

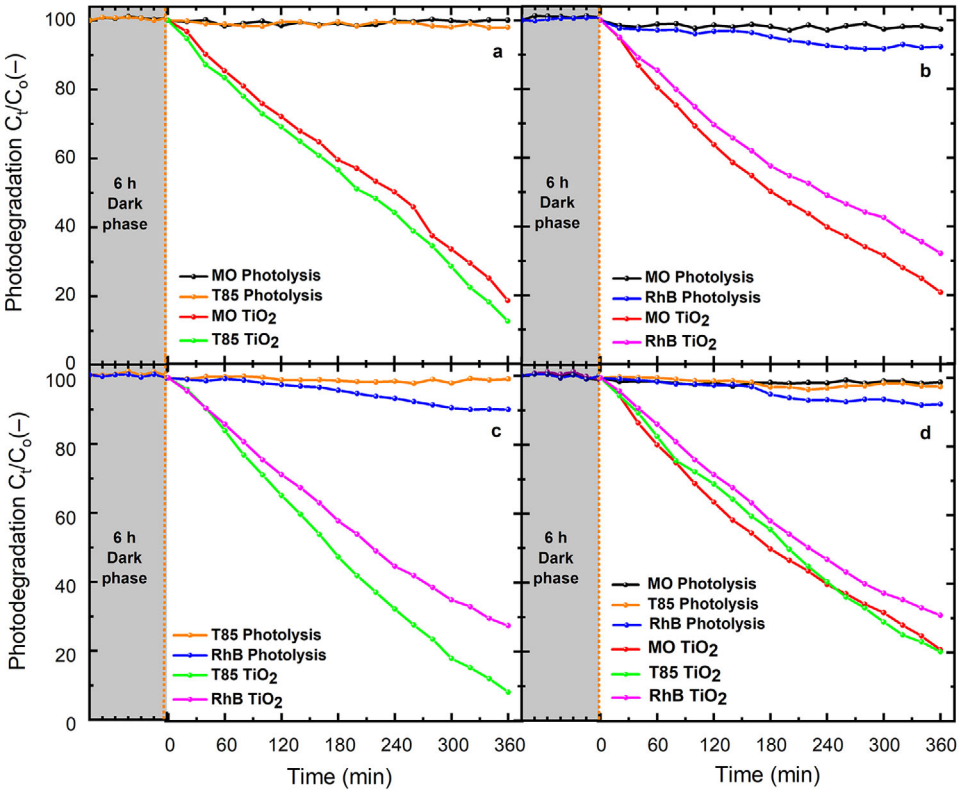

Figure 12. Photodegradation efficiency in the dark (ALD-TiO_2 thin films annealed at 600 °C) and due to photolysis and photocatalytic ALD-TiO_2 thin films (600 °C) on the mixed dye (0.01 mM) solution after 360 min of a) MO+T85 b) MO + RhB, c) T85 + RhB, each of 10 mL and (d) MO +T85 + RhB, each of 6.5 mL. Single run measurement.

The evaluation of photodegradation performance was based on the integrated absorbance bands of each dye component based on the absorption wavelength range. The results indicate that the photodegradation due to photolysis is about 2% for MO, 2% for T85, and 8% for RhB across all sets of mixed dyes. In contrast, the photocatalytic results show significant dye removal of 78% for MO and 82% for T85 in the MO + T85 (Figure 12a), 75% for MO and 65% for RhB in the MO + RhB (Figure 12b) and 86% for T85 and 70% for RhB in the T85 + RhB (Figure 12c). Additionally, in the MO + T85 + RhB (Figure 12d), the removals are 80% for MO, T85 and 70% for RhB, all after 360 min of exposure. These removal percentages are comparable to those observed for single-component dyes degraded with TiO_2 films annealed at temperatures between 400 and 650 °C presented above. Furthermore, photocatalytic tests conducted in the dark revealed no detectable degradation efficiency after 6 h, indicating removal is primarily driven via photocatalysis.

3.4.3. Photocatalytic Performance of Alternate Photocatalytic Thin Films

To evaluate the performance of FaS-PhoReS beyond TiO_2-based photocatalysts, zinc oxide (ZnO) thin films were coated onto 20 × 20 mm fused silica substrates using the molecular precursor method (MPM). This coating technique has been previously described by one of the authors.[69] The films were annealed at 500 °C for 1 h in air and had a thickness of 60 nm. The photocatalytic activity of the films was evaluated through the photodegradation of MO, DB85, T85 and RhB dye aqueous solutions, that is, the same tests as those conducted with ALDTiO_2 films in Section 2.6. The measured absorbance spectra recorded over a 360 min period with ZnO photocatalysts present are displayed in **Figure 13**. As illustrated, there is a significant decrease in absorption bands for MO (Figure 13a) and T85 (Figure 13c), while the changes observed for DB85 (Figure 13b) and RhB (Figure 13d) are moderate over time. It is also interesting to note an increase in absorption for the DB38 dye occurring in the 300 – 400 nm range. This is attributed to the formation of various complex intermediate compounds, such as aromatic and aliphatic, before complete mineralization into water and carbon dioxide.[70]

The quantification of the degree of photodegradation efficiencies is presented in **Figure 14**a,b. Building on the ALDTiO_2 films discussed earlier (Figure 10), the graphs here now compare the ZnO removal with TiO_2. In addition, to verify that removal is not occurring via adsorption, dark measurements were conducted for 6 h prior to turning on the solar simulator. For these experiments, the wells contained photocatalytically-coated samples in the relevant dye solutions, however, the samples were only exposed to light for a brief period once per hour to conduct the optical absorption measurements. The degree of photodegradation due to the photolysis of each of the dyes remained negligible. In the presence of ZnO and TiO_2 thin films, the photodegradation efficiency observed after 360 min was about 52% and 81%

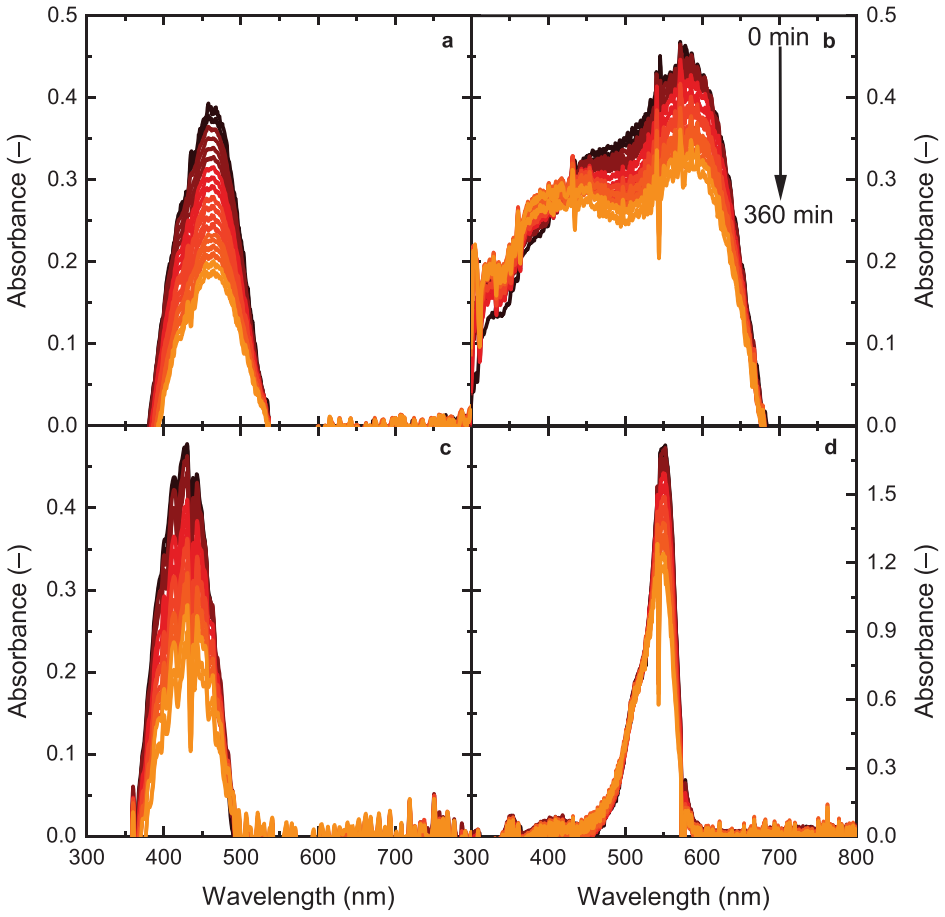

Figure 13. Photocatalysis time-dependent evolution of absorption spectra changes of anionic compounds a) MO, b) DB38, whereas cationic compounds c) T85 and d) RhB dye aqueous solution with an initial concentration of 0.01 mM after 360 min in the presence of ZnO thin films annealed at 500 °C in a single run measurement.

for MO, 17% and 50% for DB38, 55% and 90% for T85, and 21% and 66% for RhB, respectively. Despite the TiO_2 and ZnO having comparable absorption spectra and bandgap, as shown in Figures S30a,b and S31a,b, Supporting Information, respectively, the overall performance revealed that TiO_2 exhibits a superior capacity for photodegradation than ZnO. The minimal photodegradation efficiency with ZnO is due to the high recombination rate of the generated charge carriers, thus suppressing the production of the ROSs.[71] The high efficiency with TiO_2 is attributed to its indirect bandgap that increases the charge lifetime due to diffusion length, thus reducing recombination and promoting photocatalytic performance.[63,72] Additionally, the low performance of thicker ZnO films (60 nm) compared to 21. 6 nm of TO_2 is possibly attributed to the internal mass transfer of charge carriers generated from the bulk catalyst to liquid-solid interface and consequently lower the photocatalytic reaction rate.[73]

3.4.4. Photocatalytic Performance of TiO_2 Nano-Powders with Photostable Dyes using FaS-PhoReS

This section seeks to demonstrate the suitability of FaS-PhoReS to other types of photocatalysts beyond thin films. Thus, the use of TiO_2 nano-powders without the need of a magnetic stir bar for the agitating was investigated. The XRD patterns of the TiO_2 nano-powders are plotted in Figure S32, Supporting Information, indeed demonstrating the anatase phase only. Four different masses of TiO_2 nano-powders (1.0, 0.5, 0.3 and 0.1 mg) were measured using a balance and then dispersed in 20 mL of deionized water. Subsequently, a 2 mL aliquot of each sample was collected and placed into a quartz glass cuvette. The optical transmittance was then quantified using a spectrophotometer, with the cuvette being placed in the centre of the integrating sphere. The results presented in Figure S24a, Supporting Information reveal an average transmittance of 34, 55, 70 and 80% for 1.0, 0.5, 0.3, and 0.1 mg, respectively – compared to a 92% transmission through water (no TiO_2 nano-powder). The low transmittance observed in the 1.0 and 0.5 mg samples is attributed to high scattering via the particles in the suspension. However, it was deemed that the transmission of the 0.1 and 0.3 mg samples would be sufficient to study the photocatalytic degradation in FaS-PhoReS illuminated by the MH lamp. For these experiments, the 0.1 and 0.3 mg amounts were mixed into 20 mL of 0.01 mM methyl orange (MO) dye solution and dispensed into three different wells, with one well-being reserved as the control for the experiment (photolysis). Both measurements in two runs were recorded in

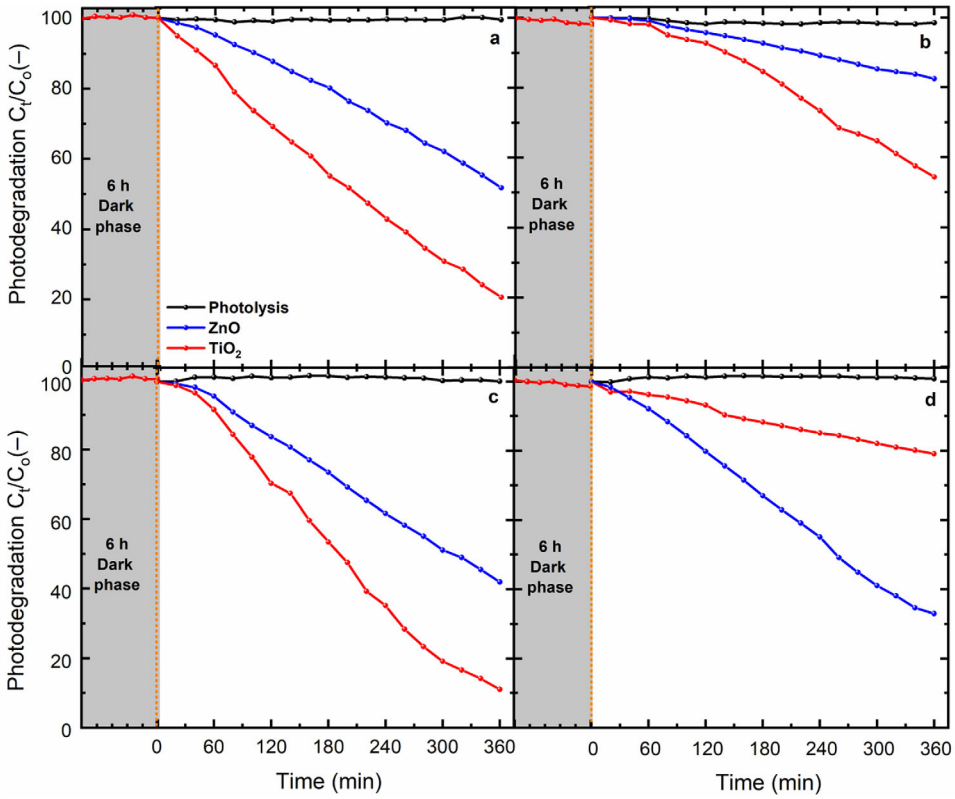

Figure 14. The degree of photodegradation in the dark (ALD-TiO_2 thin films annealed at 600 °C) as well as without and with MPM-ZnO and ALD-TiO_2 thin films both annealed at 500 °C in 20 mL of a) MO, b) DB38, c) T85, and d) RhB aqueous dye solution with an initial concentration of 0.01 mM after 360 min in a single run measurement.

intervals of 20 min for the period of 360 min of irradiation. For the photocatalytic experiment, Figure S24b,c, Supporting Information depict the light intensity transmitted through DI water and MO dye solution only (as a reference), as well as through the TiO_2 nano-powder suspensions (Figure S24d,e). The observation revealed the comparative transmittance of light intensity for all cases, with no significant change in intensity through the suspension. This clearly illustrates little agglomeration and suspension of the particles in the solution. **Figure 15**a demonstrates the decrease in absorption spectra in the 0.1 mg experiment (the results of the 0.3 mg can be found in Figure S25, Supporting Information), while Figure 15b plots the integrated photodegradation as a function of irradiation time for both loadings. The results reveal that rapid photodegradation takes place for the first 150 min in both cases, with the 0.1 mg loading resulting in slightly faster photodegradation. Then, from 180 – 360 min, the level of

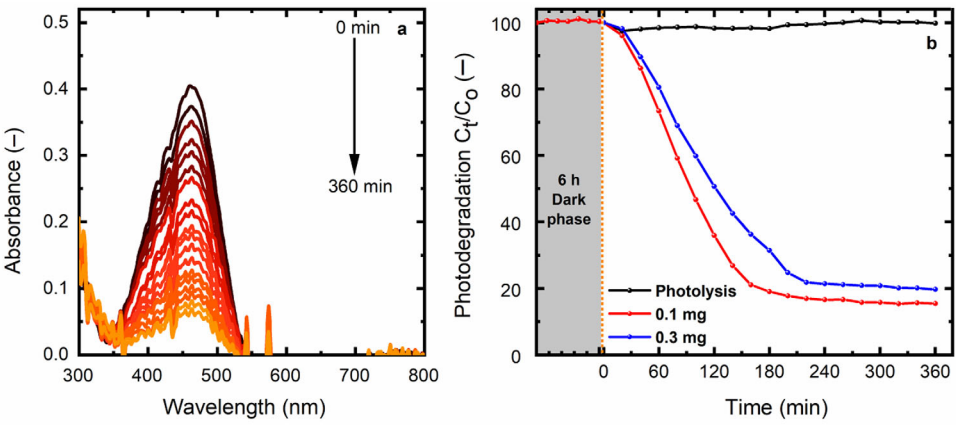

Figure 15. a) Absorption spectra of 0.1 mg TiO_2 nano-powders in 20 mL of MO (0.01 mM) dye aqueous and b) degree of photodegradation in the dark and 0.1 mg, 0.3 mg of TiO_2 nano-powders in the presence of light after 360 min. The presented results are the average of two repeats.

photodegradation appears to remain unchanged at about 80 – 84%. The plateau in Figure 15b ≈180 min is because of light scattering and being lost from the system – not absorbed. The high photodegradation in 0.1 mg (high light transmittance – less scattering) is attributed to the presence of enough active sites of TiO_2 that absorb more dye molecules and light energy.[74] On the other hand, the low performance in 0.3 mg is probably limited by the aggression of huge particles in the slurry solution, which reduces the interfacial contact area between the dye molecules and the surface of the photocatalysts as well as the light penetration blockage, thus reducing the photodegradation.[75] Additionally, the dose below the optimal loading is limited by the number of photons absorbed because of inadequate active sites.[74b,75a] The overall results reveal that FaS-PhoReS could also work with suspensions of nano-powder that exhibit less blockage of light intensity through it.

3.5. Detection of Reactive Oxygen Species

Hydroxyl (•OH) radical and superoxide ($^{\bullet}O_2^-$) anions are among the strongest ROS generated when the photocatalysts interact with photons in the presence of either water or molecular oxygen (or both of these). Several techniques have been employed for the demonstration of ROS detection.[2] Thus, the question addressed here is to ascertain whether FaS-PhoReS – in addition to being used for determining photolytic and photocatalytic degradation – can also be used as an in situ probe of the generated •OH radicals and $^{\bullet}O_2^-$ anions. The ROS detection experiment is conducted via the photocatalytic degradation of nitroblue tetrazolium (NBT) and coumarin (Cou), which are probes for the $^{\bullet}O_2^-$ anions and •OH radicals, respectively. The photocatalytic reaction between NBT with $^{\bullet}O_2^-$ anions[76] and Cou with •OH radicals[77] in aqueous solution are presented in Figure S26a,b, Supporting Information, respectively. These organic compounds were chosen to detect ROS since they have no absorption at the excitation wavelength for photocatalysts. Similar to other experiments, 20 mL of Cou and NBT aqueous solutions of an initial concentration of 0.01 mM were distributed into six different PS wells in FaS-PhoReS subjected to MH lamp irradiation. The silica coated with ALDTiO_2 thin films (annealed at 600 ^{0}C in air for 1 h) and uncoated were both placed into four different wells, while the other two were kept for the photolysis, both illuminated for 360 min. The uncoated silica substrates and direct photolysis for control tests exhibited the same degree of photodegradation.

Figure 16a,b illustrates the photolysis and photocatalysis absorption spectra, while Figure 16c shows the photodegradation of NBT aqueous solution without and with the TiO_2 photocatalyst, respectively. The absorbance spectra results indicate nearly no photodegradation under direct photolysis, while a gradual decrease in bands was observed using ALDTiO_2 films subjected to light. Dropping of the absorbance spectra of NBT solution through the course of photocatalytic indicating production of $^{\bullet}O_2^-$ ions during the photocatalytic reaction. The results reveal a negligible degree of photodegradation via direct photolysis after 360 min of light irradiation and the NBT solution remained unchanged in colour (yellowish – initial colour) as shown in Figure 16d, while uncoated silica indicates no change in colour, as depicted in Figure 16e. However, via photocatalysis, ≈18% removal is achieved and after 360 min the colour of the NBT solution changed to brown (Figure 16f) while silica-coated TiO_2 thin films changed to brown/dark (Figure 16g) due to the formation of formazan on its surface.[2] The colour change of the silica TiO_2 film is attributed to the reduction of NBT by $^{\bullet}O_2^-$ from photo-irradiated TiO_2.[2] It also noted the formation of gas bubbles on the well due to the course of the photocatalytic process.[78] The bubbling gas indicates the formation of formazan from NBT after being reduced by $^{\bullet}O_2^-$ ions.[76] These findings confirmed the presence of $^{\bullet}O_2^-$ that is produced from the reduction of molecular oxygen with an electron from photo-irradiated TiO_2 by photons with sufficient energy. The observation is in agreement with reports in the literature whereby the NBT yellow colour changed to brown/dark-blue formazan by $^{\bullet}O_2^-$ generated from photo-illuminated TiO_2.[2,76,78a] From this observation, it was confirmed that no formazan was produced from the control test but only produced photocatalytically in the presence of $^{\bullet}O_2^-$ ions.

For the photodegradation of Cou as a •OH radical probe, both photolysis and photocatalysis are shown in **Figure 17**a. The absorption reduction rate of the Cou during photocatalysis (Figure S27a, Supporting Information) indicates no significant decrease in spectra, which displays a similar trend under direct photolysis (Figure S27b, Supporting Information) over the entire period of illumination. The degradation efficiency indicates about 15% and 25% removal during the photolytic and photocatalytic process, respectively. This could be due to the significant amount of incident UV photons being absorbed by the Cou molecules in aqueous solution, greatly limiting the number of these exciting TiO_2 photocatalysts. The limited number of photons on the photocatalyst surface promotes insufficient generation of the •OH radicals. This leads to minimal removal of Cou and low yields of fluorescent 7-OHC produced after the reaction of Cou aqueous solutions with •OH radicals generated by photoexcited TiO_2.[79] The poor photocatalytic degradation leads to inefficient detection of generated 7-OHC by FaS-PhoReS. To confirm the presence •OH radical, Cou solutions before and after photocatalytic degradation were measured by FS5 Spectrofluorometer. The fluorescence signal measurements were recorded at an excitation band of 275 nm in a range of 300 to 600 nm at a slit of 1 mm (both excitation and emission). Figure 17b illustrates the fluorescence intensity of the compounds produced before and after 360 min of irradiation to the Cou solution with TiO_2 thin film. The results indicate a fluorescence emission peak of 7-OHC ≈460 nm generated after Cou reacts with •OH from photo-illuminated TiO_2. In contrast, no fluorescence was observed before the photocatalytic reaction. This observation is comparable with the studies of McCormick et al.,[80] Leandri et al.,[81] and Manevich et al.[82] These findings justify that FaS-PhoReS is limited for the detection of the 7-OHC due to the scattering effect by the multiple layers of PS container and satin finish of the bottom glass of the sample tray.

4. Conclusions

This study introduced and validated a new high-throughput FaS-PhoReS instrument capable of processing 32 samples at the same time. The system is a highly efficient and cost-effective method for screening water-borne micropollutants and novel photocatalysts. The set-up system was tested in both environmental

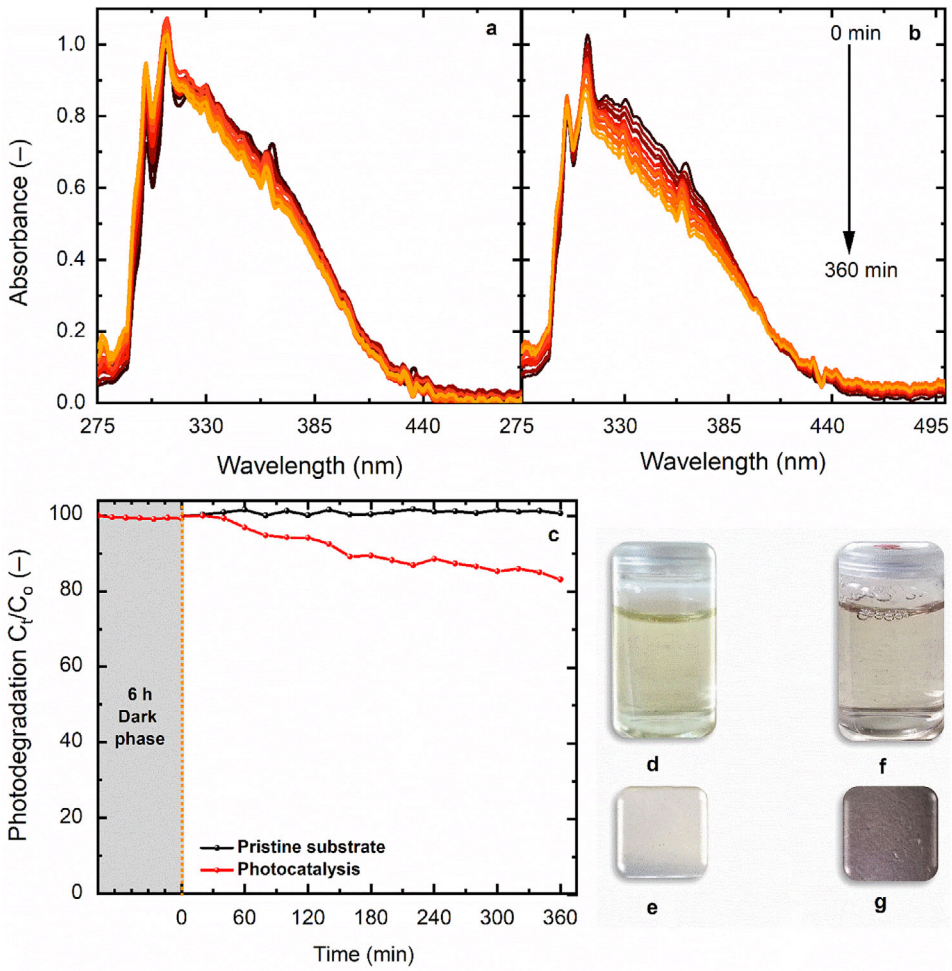

Figure 16. Time evolution of absorption spectra (20 mL NBT) due to a) photolysis and b) photocatalysis while c) photodegradation efficiency in the dark and presence of light with ALD-TiO_2 thin films annealed at 600 °C. Schematic photographs representing an illustration of no colour change of the d) NBT solution (0.01 mM) with the e) uncoated substrate and f) colour change of the NBT solution with the ALD-TiO_2 thin film g) irradiated with simulated sunlight for a period of 360 min.

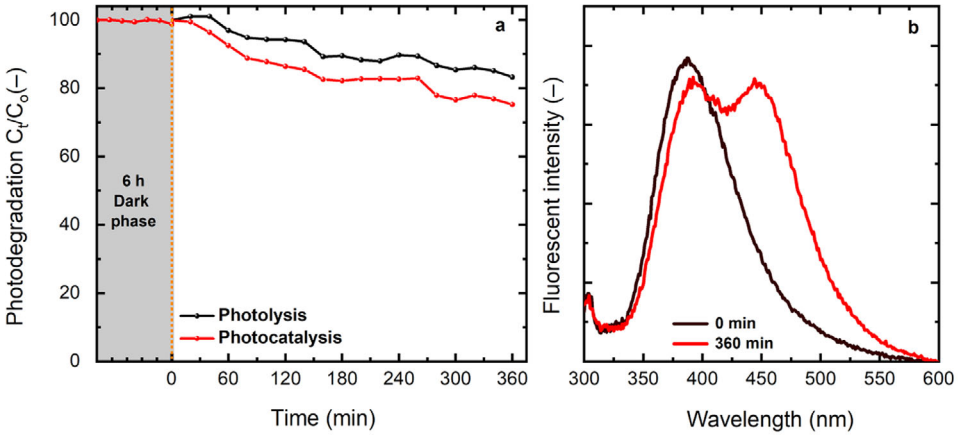

Figure 17. a) The degree of photodegradation in the dark (ALD-TiO_2 thin films annealed at 600 °C) and due to photolysis and photocatalysis (using TiO_2 film annealed at 600 °C) in 20 mL of Cou (0.01 mM) solution; b) Fluorescence emission spectra of Cou solution before and after 360 min of photocatalysis.

conditions; at controlled temperature and humidity across a wide range using a climatic chamber with the MH lamp and in uncontrolled conditions using LED. The results show significantly higher removal of MO (90%) with an MH lamp in controlled experimental conditions (23 °C and 40% RH) compared to an LED lamp (79%) under uncontrolled conditions. The high removal is attributed to more UV energy present in MH (32 mW cm^{-2}) that enhances the high excitation of TiO_2 compared to LED (3.2 mW cm^{-2}). The study validated the instrument's reliability by comparing the effects of dye evaporation, photolysis, and photocatalysis using pristine TiO_2 thin films and nanoparticles. The dye screening process using this technique demonstrated consistent results due to photolysis for the identification of the most stable organic dyes to be used in photocatalysis studies. The study found high photolysis removal for MB, U, IB, and BF, ranging from 9 to 59% while the least for RhB, DB38, MO, and T85 were between 0 and 8%. Non-degradable dyes under photolysis indicate that dyes absorb very minimal photons, and most of them penetrate the dye solution to reach the surface of the photocatalyst, leading to the true determination of photocatalytic degradation.

For the true evaluation of the activity, the photolysis experiment along with photocatalysis of the MO, T85 RhB, and DB38 with TiO_2 thin films annealed at different temperatures were studied. The photolysis results showed non-degradability for MO and T85 compared to about 9% removal for RhB and 12% for DB38 after 360 min. These findings reveal that MO and T85 are the best candidates for photodegradation studies of novel photocatalysts for the proposed system and experimental protocol. On the other hand, the photocatalysis results of TiO_2 thin films annealed at 500 to 600 °C showed superior photodegradation performance for the MO and T85, while RhB and DB38 showed moderate removal. The ZnO films exhibited satisfactory photodegradation performance for MO and T85, while the least for RhB and DB38. Additionally, FaS-PhoReS demonstrated its robustness in screening the TiO_2 nano-powders without the requiring stirring and prior filtration of solution after photodegradation before absorbance measurements. Dosages between 0.1 and 0.3 mg provided good transmittance of light intensity with minimal blockage. This is because nano-powders were suspended in a solution without aggregate and agglomerate at the bottom of the wells, which can block the optical fibers from sensing the signals. Moreover, the system demonstrated the photodegradation of different mixed dye solutions. The results reveal that the technique is capable of detecting the absorption band of each dye component present in the mixed solutions. Furthermore, FaS-PhoReS successfully detected $^{\bullet}O_2^-$ ions, but •OH radicals were not detected due to minimal photon penetration, leading to low production of 7-OHC. The fluorescent signals of 7-OHC are likely scattered by the multiple layers of the tray sample, thus the weak signals to the optical fibre sensor. Overall, the study highlighted the robustness and versatility of FaS-PhoReS in advancing photocatalytic research and its potential as a powerful tool for high-throughput screening of novel photocatalysts and pollutants. Additionally, the system is suitable to work with any photocatalysts that absorb photons in the 300–1100 nm range of light source powering the FaS-PhoReS. Similarly, pollutants that exhibit absorption in that range will function, while less than 300 nm will not be possible due to limited range.

Supporting Information

Supporting Information is available from the Wiley Online Library or from the author.

Acknowledgements

The authors gratefully acknowledge financial support from the following sources: i) the DFG "SolPhoWat" project (number 462474107) (B.S.R. and A.T.); ii) the World Bank collaboration with the Dar es Salaam University College of Education via Higher Education for Economic Transformation (HEET) Project for providing a PhD scholarship to E.M.M.; iii) the Ministry of Science, Research and Arts (MWK) of Baden-Württemberg for funding the SPheRe project (B.S.R.) that enabled L.S.D. to undertake an extended research stay at KIT in 2023; and iv) the Helmholtz Association – Research Field Energy – Materials and Technologies for the Energy Transition program (Topic 1 Photovoltaics and Wind Energy, 38.01.05).

Conflict of Interest

The authors declare no conflict of interest.

Data Availability Statement

The data that support the findings of this study are available from the corresponding author upon reasonable request.

Keywords

high-throughput screening, in-operando characterisation, photocatalysis, photocatalytic reactor system, photolysis

Received: December 13, 2024
Revised: March 20, 2025
Published online: May 19, 2025

[1] a) M. O. Barbosa, N. F. Moreira, A. R. Ribeiro, M. F. Pereira, A. M. Silva, *Water Res.* **2016**, *94*, 257; b) Y. Yang, X. Zhang, J. Jiang, J. Han, W. Li, X. Li, K. M. Yee Leung, S. A. Snyder, P. J. Alvarez, *Environ. Sci. Technol.* **2021**, *56*, 13; c) L. Sima, J. Amador, A. K. Da Silva, S. M. Miller, A. N. Morse, M.-L. Pellegrin, C. Rock, M. J. M. Wells, *Water Environ. Res.* **2014**, *86*, 1994.
[2] Y. Nosaka, A. Y. Nosaka, *Chem. Rev.* **2017**, *117*, 11302.
[3] F. Fresno, R. Portela, S. Suárez, J. M. Coronado, *J. Mater. Chem. A* **2014**, *2*, 2863.
[4] a) a. ahmadpour, *Adv. Environ. Technol.* **2015**, *1*, 121; b) Z. A. Mohd Hir, A. H. Abdullah, Z. Zainal, H. N. Lim, *J. Mater. Sci.* **2018**, *53*, 13264; c) K. Thompson, J. Goodall, S. Kellici, J. A. Mattinson, T. A. Egerton, I. Rehman, J. A. Darr, *J. Chem. Technol. Biotechnol.* **2009**, *84*, 1717.
[5] a) C. Lettmann, H. Hinrichs, W. F. Maier, *Angew. Chem., Int. Ed.* **2001**, *40*, 3160; b) J. M. Sohn, K. S. Oh, S. I. Woo, *Korean J. Chem. Eng.* **2004**, *21*, 123; c) L. S. Daniel, H. Nagai, N. Yoshida, M. Sato, *Catalysts* **2013**, *3*, 625; d) S. J. Pollack, J. W. Jacobs, P. G. Schultz, *Science* **1986**, *234*, 1570.
[6] G. Collazzo, S. Jahn, E. Foletto, *Lat. Am. Appl. Res.* **2012**, *42*, 55.
[7] a) R. A. Lerner, S. J. Benkovic, P. G. Schultz, *Science* **1991**, *252*, 659; b) A. Tramontano, K. D. Janda, R. A. Lerner, *Science* **1986**, *234*, 1566; c) S. P. A. Fodor, J. L. Read, M. C. Pirrung, L. Stryer, A. T. Lu, D. Solas,

Science **1991**, *251*, 767; d) R. A. Houghten, C. Pinilla, S. E. Blondelle, J. R. Appel, C. T. Dooley, J. H. Cuervo, *Nature* **1991**, *354*, 84; e) R. N. Motz, E. M. Lopato, T. U. Connell, S. Bernhard, *Inorg. Chem.* **2021**, *60*, 774.

[8] a) T. B. Engelhardt, S. Schmitz-Stöwe, T. Schwarz, K. Stöwe, *ChemistryOpen* **2022**, *11*, 202200180; b) C. Lin, X. Feng, D. Legut, X. Liu, Z. W. Seh, R. Zhang, Q. Zhang, *Adv. Funct. Mater.* **2022**, *32*, 2207415; c) M. A. Behnajady, N. Modirshahla, M. Shokri, *Chemosphere* **2004**, *55*, 129; d) K. Yanagiyama, K. Takimoto, S. Dinh Le, N. Nu Thanh Ton, T. Taniike, *Environ. Pollut.* **2024**, *342*, 122974; e) X.-D. Xiang, X. Sun, G. Briceño, Y. Lou, K.-A. Wang, H. Chang, W. G. Wallace-Freedman, S.-W. Chen, P. G. Schultz, *Science* **1995**, *268*, 1738.

[9] J. Ding, J. Bao, S. Sun, Z. Luo, C. Gao, *J. Comb. Chem.* **2009**, *11*, 523.

[10] a) N. Qi, M. K. Wismer, D. V. Conway, S. W. Krska, S. D. Dreher, S. Lin, *React. Chem. Eng.* **2022**, *7*, 354; b) S. I. Woo, K. W. Kim, H. Y. Cho, K. S. Oh, M. K. Jeon, N. H. Tarte, T. S. Kim, A. Mahmood, *QSAR Comb. Sci.* **2005**, *24*, 138; c) S. Sun, J. Ding, J. Bao, Z. Luo, C. Gao, *Comb. Chem.* **2011**, *14*, 160; d) Y. Zhao, J. Gao, X. Bian, H. Tang, T. Zhang, *Green Energy Environ.* **2024**, *9*, 1; e) J. Romão, D. Barata, N. Ribeiro, P. Habibovic, H. Fernandes, G. Mul, *Environ. Pollut.* **2017**, *220*, 1199; f) S. K. Kansal, M. Singh, D. Sud, *J. Hazard. Mater.* **2007**, *141*, 581.

[11] H. Issa Hamoud, L. Wolski, I. Pankin, M. A. Bañares, M. Daturi, M. El-Roz, *Top. Curr. Chem.* **2022**, *380*, 37.

[12] J. M. Coronado, F. Fresno, A. Iglesias-Juez, in *Materials Science in Photocatalysis*, (Eds: E. I. García-López, L. Palmisano), Elsevier, Amsterdam **2021**.

[13] A. Peter, A. Mihaly-Cozmuta, C. Nicula, L. Mihaly-Cozmuta, A. Jastrzębska, A. Olszyna, L. Baia, *Water, Air, Soil Pollut.* **2016**, *228*, 41.

[14] A. Mills, *Appl. Catal., B* **2012**, *128*, 144.

[15] a) B. Ohtani, *J. Photochem. Photobiol., C* **2010**, *11*, 157; b) S. Bae, S. Kim, S. Lee, W. Choi, *Catal. Today* **2014**, *224*, 21; c) A. Mills, J. Wang, *J. Photochem. Photobiol., A* **1999**, *127*, 123.

[16] a) X. Yan, T. Ohno, K. Nishijima, R. Abe, B. Ohtani, *Chem. Phys. Lett.* **2006**, *429*, 606; b) F. R. Amalia, M. Takashima, B. Ohtani, *Chem. Commun.* **2022**, *58*, 11721.

[17] N. Barbero, D. Vione, *Environ. Sci. Technol.* **2016**, *50*, 2130.

[18] H. Schmidt, M. Akarsu, T. S. Müller, K. Moh, G. Schäfer, D. J. Strauss, M. Naumann, *Res. Chem. Intermed.* **2005**, *31*, 535.

[19] T. F. Jaramillo, S.-H. Baeck, A. Kleiman-Shwarsctein, K.-S. Choi, G. D. Stucky, E. W. McFarland, *J. Comb. Chem.* **2005**, *7*, 264.

[20] A. Nakayama, E. Suzuki, T. Ohmori, *Appl. Surf. Sci.* **2002**, *189*, 260.

[21] M. Seyler, K. Stoewe, W. F. Maier, *Appl. Catal., B* **2007**, *76*, 146.

[22] H. Y. Xiao, Q. X. Dai, W. S. Li, C. T. Au, X. P. Zhou, *J. Mol. Catal. A: Chem.* **2006**, *245*, 17.

[23] M. Zhang, J. Lee, L. Wang, Q. Duan, J. Zhang, H. Qi, *ChemCatChem* **2015**, *7*, 3978.

[24] J. Romão, D. Barata, P. Habibovic, G. Mul, J. Baltrusaitis, *Anal. Chem.* **2014**, *86*, 7612.

[25] Y. Bi, P. Westerhoff, *Chemosphere* **2019**, *223*, 275.

[26] N. D. Morris, T. E. Mallouk, *J. Am. Chem. Soc.* **2002**, *124*, 11114.

[27] International Electrotechnical Commission (IEC) Standard 60068-2-5, Geneva 2018

[28] a) R. Lyubimenko, A. Turshatov, A. Welle, P. G. Weidler, B. S. Richards, A. I. Schäfer, *Chem. Eng. J.* **2023**, *451*, 138449; b) T. E. Berger, C. Regmi, A. I. Schäfer, B. S. Richards, *J. Membr. Sci.* **2020**, *604*, 118015.

[29] I. Groeneveld, M. Kanelli, F. Ariese, M. R. van Bommel, *Dyes Pigm.* **2023**, *210*, 110999.

[30] A. Godoy Junior, A. Pereira, M. Gomes, M. Fraga, R. Pessoa, D. Leite, G. Petraconi, A. Nogueira, H. Wender, W. Miyakawa, *Catalysts* **2020**, *10*, 282.

[31] T. Berger, C. Regmi, A. Schäfer, B. Richards, *J. Membr. Sci.* **2020**, *604*, 118015.

[32] a) J. Peral, X. Domènech, D. F. Ollis, *J. Chem. Technol. Biotechnol.* **1997**, *70*, 117; b) R. Liu, J. Wang, J. Zhang, S. Xie, X. Wang, Z. Ji, *Microporous Mesoporous Mater.* **2017**, *248*, 234; c) A. Kumar, G. Pandey, *Mater. Sci. Eng. Int. J.* **2017**, *1*, 106; d) B. Acemioğlu, *Int. J. Coal Prep. Util.* **2022**, *42*, 671.

[33] a) N. A. Barakat, M. A. Kanjwal, I. S. Chronakis, H. Y. Kim, *J. Mol. Catal. A: Chem.* **2013**, *366*, 333; b) S. Zhou, A. K. Ray, *Ind. Eng. Chem. Res.* **2003**, *42*, 6020.

[34] a) Q. Huang, W. Ma, X. Yan, Y. Chen, S. Zhu, S. Shen, *J. Mol. Catal. A: Chem.* **2013**, *366*, 261; b) T. Martinez, A. Bertron, G. Escadeillas, E. Ringot, V. Simon, *Build. Environ.* **2014**, *71*, 186; c) G. Zhang, A. Peyravi, Z. Hashisho, Z. Sun, Y. Liu, S. Zheng, L. Zhong, *Catal. Sci. Technol.* **2020**, *10*, 2378.

[35] a) J. S. Kim, T. K. Lee, *Korean J. Chem. Eng.* **2001**, *18*, 935; b) S. Saqlain, B. J. Cha, S. Y. Kim, J. Y. Sung, M. C. Choi, H. O. Seo, Y. D. Kim, *Mater. Today Commun.* **2021**, *26*, 102119.

[36] T. Bouarroudj, L. Aoudjit, L. Djahida, B. Zaidi, M. Ouraghi, D. Zioui, S. Mahidine, C. Shekhar, K. Bachari, *Water Sci. Technol.* **2021**, *83*, 2118.

[37] H. V. BEEK, P. M. Heertjes, *Stud. Conserv.* **1966**, *11*, 123.

[38] a) G. Wei, C. Basheer, C.-H. Tan, Z. Jiang, *Tetrahedron Lett.* **2016**, *57*, 3801; b) A. Enesca, L. Andronic, A. Duta, *Catal. Lett.* **2012**, *142*, 224.

[39] G. K. Gupta, M. K. Mondal, in *Photocatalytic Degradation of Dyes*, (Eds: M. Shah, S. Dave, J. Das), Elsevier, Amsterdam **2021**.

[40] C. Joseph, Y. H. Taufiq-Yap, L. Elilarasi, V. Krishnan, *Malays. J. Chem.* **2017**, *19*, 82.

[41] S. Kader, M. R. Al-Mamun, M. B. K. Suhan, S. B. Shuchi, M. S. Islam, *Environ. Technol. Innovation* **2022**, *27*, 102476.

[42] S. Boukhedoua, R. Zouaghi, O. N. E. H. Kaabeche, *Int. J. Chem. Reactor Eng.* **2022**, *20*, 735.

[43] H. Bendjama, S. Merouani, O. Hamdaoui, M. Bouhelassa, *J. Photochem. Photobiol., A* **2019**, *368*, 268.

[44] N. Guettaï, H. A. Amar, *Desalination* **2005**, *185*, 427.

[45] Q. Hu, B. Liu, z. Zhang, M. Song, X. Zhao, *J. Wuhan Univ. Technol. Mater. Sci. Ed.* **2010**, *25*, 210.

[46] M. Utami, S. Wang, F. I. Fajarwati, S. N. Salsabilla, T. A. Dewi, M. Fitri, *Crystals* **2023**, *13*, 588.

[47] F. Alakhras, E. Alhajri, R. Haounati, H. Ouachtak, A. A. Addi, T. A. Saleh, *Surf. Interfaces* **2020**, *20*, 100611.

[48] P. H. Allé, G. D. Fanou, D. Robert, K. Adouby, P. Drogui, *Appl. Water Sci.* **2020**, *10*, 207.

[49] J. R. Guimarães, M. Guedes Maniero, R. Nogueira de Araújo, *J. Environ. Manage.* **2012**, *110*, 33.

[50] T. Soltani, M. H. Entezari, *J. Mol. Catal. A: Chem.* **2013**, *377*, 197.

[51] S. Bendjabeur, R. Zouaghi, B. Zouchoune, T. Sehili, *Spectrochim. Acta, Part A* **2018**, *190*, 494.

[52] a) R. Hussin, K. L. Choy, X. H. Hou, *Adv. Mater. Res.* **2016**, *1133*, 352; b) C. Jin, B. Liu, Z. Lei, J. Sun, *Nanoscale Res. Lett.* **2015**, *10*, 95; c) J. Aarik, A. Aidla, A.-A. Kiisler, T. Uustare, V. Sammelselg, *Thin Solid Films* **1997**, *305*, 270.

[53] C.-S. Lee, J. Kim, J. Y. Son, W. Choi, H. Kim, *Appl. Catal., B* **2009**, *91*, 628.

[54] C.-H. Hsu, K.-T. Chen, P.-H. Huang, W.-Y. Wu, X.-Y. Zhang, C. Wang, L.-S. Liang, P. Gao, Y. Qiu, S.-Y. Lien, *Nanomaterials* **2020**, *10*, 1322.

[55] V. S. Dang, H. Parala, J. H. Kim, K. Xu, N. B. Srinivasan, E. Edengeiser, M. Havenith, A. D. Wieck, T. de los Arcos, R. A. Fischer, *Phys. Status Solidi A* **2014**, *211*, 416.

[56] R. Pheamhom, C. Sunwoo, D.-H. Kim, *J. Vac. Sci. Technol., A* **2006**, *24*, 1535.

[57] K. Eufinger, D. Poelman, H. Poelman, R. De Gryse, G. Marin, *Thin Solid Films* **2008**, *37661*, 2.

[58] S. B. Amor, L. Guedri, G. Baud, M. Jacquet, M. Ghedira, *Mater. Chem. Phys.* **2003**, *77*, 903.

[59] C.-S. Lee, J. Kim, J. Son, W. Choi, H. Kim, *Appl. Catal., B* **2009**, *91*, 628.

[60] I. J. Badovinac, R. Peter, A. Omerzu, K. Salamon, I. Šarić, A. Samaržija, M. Perčić, I. K. Piltaver, G. Ambrožić, M. Petravić, *Thin Solid Films* **2020**, *709*, 138215.

[61] G. Liu, F. Shan, W. Lee, B. Shin, *J. Korean Phys. Soc.* **2007**, *50*, 1827.
[62] B. S. Richards, *Sol. Energy Mater. Sol. Cells* **2003**, *79*, 369.
[63] A. Fujishima, T. N. Rao, D. A. Tryk, *J. Photochem. Photobiol., C* **2000**, *1*, 1.
[64] M. Schiavello,*Heterogeneous Photocatalysis*, Wiley, Hoboken **1997**.
[65] a) H. Kisch, *Semiconductor Photocatalysis: Principles and Applications*, John Wiley & Sons, Hoboken **2015**; b) O. Carp, C. L. Huisman, A. Reller, *Prog. Solid State Chem.* **2004**, *32*, 33.
[66] F. Dufour, S. Pigeot-Remy, O. Durupthy, S. Cassaignon, V. Ruaux, S. Torelli, L. Mariey, F. Maugé, C. Chanéac, *Appl. Catal., B* **2015**, *174*, 350.
[67] M. Behnajady, N. Modirshahla, M. Shokri, B. Rad, *Global NEST J.* **2008**, *10*, 1.
[68] N. Riaz, M. Hassan, M. Siddique, Q. Mahmood, U. Farooq, R. Sarwar, M. S. Khan, *Environ. Sci. Pollut. Res.* **2020**, *27*, 2992.
[69] T. Amakali, L. S. Daniel, V. Uahengo, N. Y. Dzade, N. H. De Leeuw, *Crystals* **2020**, *10*, 132.
[70] S. K. Abbas, Z. M. Hassan, L. M. Ahmed, *J. Phys.: Conf. Ser.* **2019**, *1294*, 052050.
[71] Y. Liao, C. Xie, Y. Liu, H. Chen, H. Li, J. Wu, *Ceram. Int.* **2012**, *38*, 4437.
[72] W. Fu, G. Li, Y. Wang, S. Zeng, Z. Yan, J. Wang, S. Xin, L. Zhang, S. Wu, Z. Zhang, *Chem. Commun.* **2018**, *54*, 58.
[73] D. Chen, F. Li, A. K. Ray, *Catal. Today* **2001**, *66*, 475.
[74] a) F. Azeez, E. Al-Hetlani, M. Arafa, Y. Abdelmonem, A. A. Nazeer, M. O. Amin, M. Madkour, *Sci. Rep.* **2018**, *8*, 7104; b) S. L. N. Zulmajdi, N. I. I. Zamri, H. M. Yasin, E. Kusrini, J. Hobley, A. Usman, *React. Kinet., Mech. Catal.* **2020**, *129*, 519.
[75] a) H. Coleman, V. Vimonses, G. Leslie, R. Amal, *J. Hazard. Mater.* **2007**, *146*, 496; b) Y. J. Jang, C. Simer, T. Ohm, *Mater. Res. Bull.* **2006**, *41*, 67; c) S. Anandan, P. S. Kumar, N. Pugazhenthiran, J. Madhavan, P. Maruthamuthu, *Sol. Energy Mater. Sol. Cells* **2008**, *92*, 929.
[76] H. Goto, Y. Hanada, T. Ohno, M. Matsumura, *J. Catal.* **2004**, *225*, 223.
[77] K.-i. Ishibashi, A. Fujishima, T. Watanabe, K. Hashimoto, *Electrochem. Commun.* **2000**, *2*, 207.
[78] a) L. Ye, J. Liu, Z. Jiang, T. Peng, L. Zan, *Appl. Catal., B* **2013**, *142*, 1; b) X. He, S. Sanders, W. G. Aker, Y. Lin, J. Douglas, H.-m. Hwang, *J. Environ. Sci.* **2016**, *42*, 50.
[79] a) H. Czili, A. Horváth, *Appl. Catal., B* **2008**, *81*, 295; b) T. Fotiou, T. M. Triantis, T. Kaloudis, K. E. O'Shea, D. D. Dionysiou, A. Hiskia, *Water Res.* **2016**, *90*, 52.
[80] W. J. McCormick, C. Rice, D. McCrudden, N. Skillen, P. K. Robertson, *J. Phys. Chem. A* **2023**, *127*, 5039.
[81] V. Leandri, J. M. Gardner, M. Jonsson, *J. Phys. Chem. C* **2019**, *123*, 6667.
[82] Y. Manevich, K. D. Held, J. E. Biaglow, *Radiat. Res.* **1997**, *148*, 580.